CONTROLLED OPTICAL SOLITON PROPAGATION USING THEORETICAL TUNABLE DISPERSION FIBERS

BY

THADDEUS EGON KOEHN

THESIS

Submitted in partial fulfillment of the requirements
for the degree of Master of Science in Electrical and Computer Engineering
in the Graduate College of the
University of Illinois at Urbana-Champaign, 2009

Urbana, Illinois

Adviser:

Assistant Professor Cédric Langbort

ABSTRACT

The increased demand for high bandwidth communication channels has raised significant interest in overcoming the data rate limitations of fiber communication systems. In this thesis a solution is proposed: controlled soliton propagation. This solution requires the use of new technology in the form of tunable dispersion fibers that can be tuned quickly and continuously. Assuming such a fiber can be created, control is applied so as to produce Gaussian pulses that overcome current fiber limitations by balancing dispersion and nonlinearity. The pulses will experience no dispersion on average and thus allow ultra-short pulse widths to be propagated. Simulated results suggest that this solution may succeed in propagating ultra-short pulses where current propagation techniques fail.

To my parents, for their love and support

TABLE OF CONTENTS

LIST OF FIGURES

LIST OF ABBREVIATIONS

NLSE	Nonlinear Schrödinger Equation
DM	Dispersion Management
ODE	Ordinary Differential Equation
EM	Electromagnetic
SVEA	Slowly Varying Envelope Approximation
PMD	Polarized Mode Dispersion

CHAPTER 1

INTRODUCTION

The trend in the communication industry has been a shift away from copper wires toward fiber optic communication lines. During the 1990s optical fibers were laid across the United States to most of the communication nodes, as it became apparent that fiber optics could deliver fast, reliable, and low cost data transfers. Today's demand for high bandwidth data networks has brought us to the limits of the current fiber communication infrastructure.

In theory all that is necessary to increase bandwidth and thus data speed is to increase the frequency with which the transmitter is turned on and off. The receiver would also need to change in order to decrease the error rate of symbol recovery (i.e., mistake a '0' for a '1'). There are many effects contributing to errors, but they are generally termed collectively as "noise." There are several methods for combating noise: changing the receiver and transmitter to reduce their contributions; using higher grade fibers; using a wavelength of light that is less affected by noise; and applying signal processing techniques after reception to recover the original signal. Signal processing has shown great success in combating noise, but relies on techniques that are only valid for linear systems. As the frequency regime shifts from the gigahertz to the terahertz data rates, light propagation can no longer can be approximated by purely linear effects and new technology is needed.

The phenomenon of light propagation in a fiber is generally described by the nonlinear Schrödinger equation (NLSE), which is a partial differential equation describing waves in a medium. The NLSE has three parameters used to describe the medium: β, γ, and α, corresponding to the dispersion, nonlinearity, and loss,

respectively. The effect of the nonlinearity is greater at higher frequencies and invalidates approaches that use linear models.

The soliton has received much attention as a possible solution to this problem. Originally a theoretical solution of the NLSE, a soliton is a localized wave that maintains its shape exactly without pulse or spectral broadening in an ideal lossless fiber [1]. This corresponds to a perfect balancing between the dispersion and nonlinear optical effects. The absence of broadening is desirable since it reduces communication errors in demodulation, as no inter-symbol interference occurs [2]. In practice, such balancing cannot be completely realized in the presence of attenuation. The tendency to balance without complete balancing is a physical phenomenon; pulses that behave this way are said to experience the *soliton effect*.

In 1980 at Bell Laboratories, Mollenauer, Stolen and Gordon experimentally verified the existence of a soliton [3]. This experiment worked by modifying the input pulse shape; the desired output is the input pulse. The input is tuned by output feedback to obtain a soliton. In practice fiber properties are not well known, especially the nonlinear and dispersion coefficients, and thus even if the proper pulse shape were obtained, it would propagate as a soliton only for a small section of the fiber until the fiber's properties varied too much. The current industrial choice for obtaining a similar result is *dispersion management* (DM). DM uses alternating length of positive and negative dispersion fibers to keep the pulse width within a certain tolerance. While traveling through the positive fiber the pulse width expands; it then contracts through the negative fiber until it is restored to the initial width, at which point the system is repeated. DM accounts for nonlinearity, but the spliced lengths of fiber fail to attain the required resolution needed to balance the high nonlinearity experienced by ultra-short pulse widths. Current research in the propagation of solitons involves pre-shaping the input pulse using adaptive techniques [4], [5]. Treating the fiber as an input to output map, if the inverse of this map can be found then the proper input to the fiber can be calculated as a function of the

desired output.

Recent technical developments in materials science [6] have enabled the production of tunable dispersion materials. This presents the possibility, at least in principle, of varying the dispersion map continuously over the length of the fiber using closely spaced sections of tunable dispersion material. Each discrete sections of fiber would be controlled individually, allowing a desired dispersion to be selected. The fiber's dispersion would be controlled in space rather than in time. Such a fiber would open the door to controlled dispersion management using feedback, provided that pulse broadening is measurable, and that the dispersion can be tuned fast enough.

This thesis considers such a theoretical fiber and employs it as a means of creating solitons for any pulse width, thus providing a solution for data communication. A model for light wave propagation in a fiber is developed from the foundation of Maxwell's equations to describe the dynamics of the pulse width. In Chapter 6 two control laws are developed that demonstrate the creation of a soliton, with and without chirp. These theoretical results are compared in Chapter 7 to current fiber communication techniques.

CHAPTER 2

MODEL DEVELOPMENT

Maxwell's equations are considered the de facto first principles of electricity and magnetism. From these equations the NLSE is derived. Then, using the variational approach, an ansatz describing an envelope equation is assumed. This allows the construction of a second order ODE describing the dynamics of the pulse width. This approach has been experimentally verified and is shown to be one of the best of the current models for describing light propagation [1].

2.1 The NLSE

The derivation of the NLSE from Maxwell's equation will roughly follow the derivation by Agrawal [7]. In differential form Maxwell's equations are:

$$\vec{\nabla} \times \vec{E} = -\mu_0 \frac{\partial \vec{H}}{\partial t}, \tag{2.1}$$

$$\vec{\nabla} \times \vec{H} = \frac{\partial}{\partial t}(\epsilon_0 \vec{E} + \vec{P}), \tag{2.2}$$

$$\vec{\nabla} \bullet \vec{H} = 0, \tag{2.3}$$

$$\vec{\nabla} \bullet \vec{E} = \vec{\nabla} \bullet \vec{P} = 0, \tag{2.4}$$

where $\vec{E} = \vec{E}(x, y, z, t)$ and $\vec{H} = \vec{H}(x, y, z, t)$ are the electric and magnetic fields. The constants ϵ_0 and μ_0 are the free-space *dielectric permittivity* and *magnetic permeability* respectively. The polarization vector $\vec{P} = \vec{P}(x, y, z, t)$ represents the response of the medium to the electromagnetic (EM) wave.

The polarization vector takes into account the full response of the medium to

the excitation of an incident EM field. The polarization is considered to be the superposition of both linear and nonlinear contribution, described as

$$\vec{P}(x,y,z,t) = \vec{P}_L(x,y,z,t) + \vec{P}_{NL}(x,y,z,t). \tag{2.5}$$

The specific forms of these contributions are generally determined through measurement, although some molecular models exist. One can also characterize the contribution of the material to the electric field through the electric susceptibility χ_e, defined for an instantaneous response through

$$\vec{P} = \epsilon_0 \chi_e \vec{E}. \tag{2.6}$$

In general a polarization response cannot be instantaneous, so the more general definition of polarization written as an impulse response to an electric field is

$$\vec{P}(t) = \int_{-\infty}^{\infty} \chi_e(t-\tau)\vec{E}(\tau)d\tau. \tag{2.7}$$

Models for light wave propagation in fiber are developed using Maxwell's equations in the same manner as the wave equation in free-space. The difference is due to propagation in a material which causes $\vec{P}$ to be non-zero. Taking the curl of (2.1) and then substituting in (2.2) gives

$$\begin{aligned}\vec{\nabla} \times (\vec{\nabla} \times \vec{E}) &= -\mu_0 \left(\vec{\nabla} \times \frac{\partial \vec{H}}{\partial t} \right) = -\mu_0 \frac{\partial}{\partial t}(\vec{\nabla} \times \vec{H}) = -\mu_0 \frac{\partial^2}{\partial t^2}(\epsilon_0 \vec{E} + \vec{P}) \\ &= -\epsilon_0 \mu_0 \frac{\partial^2 \vec{E}}{\partial t^2} - \mu_0 \frac{\partial^2 \vec{P}}{\partial t^2}.\end{aligned} \tag{2.8}$$

Using the vector identity $\vec{\nabla} \times (\vec{\nabla} \times \vec{E}) = \vec{\nabla}(\vec{\nabla} \bullet \vec{E}) - \nabla^2 \vec{E}$ and (2.4) results in

$$\nabla^2 \vec{E} = \epsilon_0 \mu_0 \frac{\partial^2 \vec{E}}{\partial t^2} + \frac{\mu_0 \epsilon_0}{\epsilon_0} \frac{\partial^2 \vec{P}}{\partial t^2}. \tag{2.9}$$

The standard relationship for the speed of light $\epsilon_0\mu_0 = 1/c^2$ simplifies (2.9) to

$$\nabla^2\vec{E} - \frac{1}{c^2}\frac{\partial^2\vec{E}}{\partial t^2} = \frac{1}{\epsilon_0 c^2}\frac{\partial^2\vec{P}}{\partial t^2}. \tag{2.10}$$

This is the familiar form of the wave equation in a material, where $\vec{E} = (E_x, E_y, E_y)$, $\nabla^2\vec{E} = (\nabla^2 E_x, \nabla^2 E_y, \nabla^2 E_z)$, and ∇^2 is the Laplacian operator $\nabla^2 = \frac{\partial^2}{\partial x^2} + \frac{\partial^2}{\partial y^2} + \frac{\partial^2}{\partial z^2}$. There are other version of this equation where (2.4) is not required to be zero, i.e., there is charge present in the medium [8].

In order to proceed, the polarization vector $\vec{P}$ must be more precisely considered. This is done through a series expansion of the electric susceptibility χ_e which gives the expression

$$\begin{aligned}
\vec{P}_L(\vec{r},t) &= \epsilon_0 \int_{-\infty}^{\infty} \chi^{(1)}(\vec{r}, t-\tau)\vec{E}(\vec{r},\tau)d\tau, \text{ and} \\
\vec{P}_{NL}(\vec{r},t) &= \epsilon_0 \iiint_{\Re^3} \chi^{(3)}(\vec{r}, t-\tau_1, t-\tau_2, t-\tau_3)\times \\
&\qquad \Big(\vec{E}(\vec{r},\tau_1) \bullet \vec{E}(\vec{r},\tau_2) \bullet \vec{E}(\vec{r},\tau_2)\Big)\, d\tau_1 d\tau_2 d\tau_3,
\end{aligned} \tag{2.11}$$

where $\vec{r}$ represents the spatial component (x, y, z). Notice that only the first and third terms of the susceptibility expansion are used. This is because $\chi^{(2)} = 0$ in silica (the fiber material) and the remaining higher order terms are considered to be small and are therefore ignored for the purposes of this derivation [9].

The first assumption of the derivation is that the modes are *weakly guided*. This approximation is based on the condition that the index of refraction of the cladding and core of the fiber are nearly identical, $n_1 \cong n_2$. This groups together the nearly degenerate modes. Also, it is assumed that only the fundamental mode HE_{11} propagates, i.e., the fiber is single mode. Under these assumptions the electric field $\vec{E}$ will have only one non-vanishing component and thus will reduce (2.10) and (2.11) to scaler equations, greatly reducing the complexity.

The next simplification occurs from the *slowly varying envelope approximation* (SVEA). This approximation assumes that the signal under consideration has a

central carrier frequency ω_0 and all other frequency components are concentrated near that carrier. The envelope is then described by the distribution of components around ω_0 and it slowly varies because not all components are at the carrier frequency. Solutions to (2.10) will then be of the form

$$E(x,y,z,t) = \frac{1}{2}\left(T(x,y,z,t)e^{-i\omega_0 t} + T^*(x,y,z,t)e^{i\omega_0 t}\right). \tag{2.12}$$

The complex function $T(x,y,z,t)$ is called the complex envelope of the carrier ω_0. Using the SVEA (2.12) for the electric field in (2.10) with (2.11) results in

$$\begin{aligned}\left(\nabla^2 - \frac{1}{c^2}\frac{\partial^2}{\partial t^2}\right)\left(\frac{1}{2}Te^{-i\omega_0 t} + T^*e^{i\omega_0 t}\right) = \\ \frac{1}{c^2}\frac{\partial^2}{\partial t^2}\int_{-\infty}^{\infty}\chi^{(1)}\left(\frac{1}{2}Te^{-i\omega_0\tau} + T^*e^{i\omega_0\tau}\right)d\tau \\ + \frac{1}{c^2}\frac{\partial^2}{\partial t^2}\iiint_{\Re^3}\chi^{(3)}\left(\frac{Te^{-i\omega_0\tau_1} + T^*e^{i\omega_0\tau_1}}{2}\right)\left(\frac{Te^{-i\omega_0\tau_2} + T^*e^{i\omega_0\tau_2}}{2}\right) \\ \times\left(\frac{Te^{-i\omega_0\tau_3} + T^*e^{i\omega_0\tau_3}}{2}\right)d\tau_1 d\tau_2 d\tau_3.\end{aligned} \tag{2.13}$$

The main contributions to the triple integral in (2.13) will occur when $\tau_1 \cong t$, $\tau_2 \cong t$, and $\tau_3 \cong t$, so that there is roughly a coefficient of $e^{-i\omega t}$ on the right side of (2.13). If the ways to obtain terms that contain $e^{-i\omega_0 t}$ are summed and equated to the same exponential on the right, three ways will be found: the distinct ways to write the product $(Te^{-i\omega_0 t})(Te^{-i\omega_0 t})(T^*e^{i\omega_0 t})$. After summing and equating like exponentials, the resulting equation is

$$\begin{aligned}\left(\nabla^2 - \frac{1}{c^2}\frac{\partial^2}{\partial t^2}\right)\left(Te^{-i\omega_0 t}\right) = \frac{1}{c^2}\frac{\partial^2}{\partial t^2}\int_{-\infty}^{\infty}\chi^{(1)}Te^{-i\omega_0\tau} \\ + \frac{3}{4c^2}\frac{\partial^2}{\partial t^2}\iiint_{\Re^3}\chi^{(3)}Te^{-i\omega_0\tau_1}Te^{-i\omega_0\tau_2}T^*e^{i\omega_0\tau_3}d\tau_1 d\tau_2 d\tau_3.\end{aligned} \tag{2.14}$$

Let $S(\vec{r},t) = T(\vec{r},t)e^{-i\omega_0 t}$. In terms of S, (2.14) becomes

$$\nabla^2 S - \frac{1}{c^2}\frac{\partial^2 S}{\partial t^2} = \frac{1}{c^2}\frac{\partial^2}{\partial t^2}\int_{-\infty}^{\infty}\chi^{(1)}(t-\tau)S(\tau)d\tau + \frac{3}{4c^2}\frac{\partial^2}{\partial t^2}\iiint_{\Re^3}\chi^{(3)}(\vec{t}-\vec{\tau})S(\tau_1)S(\tau_2)S^*(\tau_3)d\vec{\tau}, \tag{2.15}$$

where $\vec{t}-\vec{\tau} = (t-\tau_1, t-\tau_2, t-\tau_3)$ and the spatial variable is suppressed for simplicity.

Now consider the Fourier transform of $S(\vec{r},t)$ denoted by $\hat{S}(\vec{r},\omega)$. The transform of the left side of equation (2.15) is

$$\left(\nabla^2 + \frac{\omega^2}{c^2}\right)\hat{S}(\vec{r},\omega). \tag{2.16}$$

Denote $\hat{\chi}^{(1)}(\vec{r},\omega) = \int_{-\infty}^{\infty}\chi^{(1)}(\vec{r},t)e^{i\omega\tau}d\tau$ as the Fourier transform of the linear susceptibility. It is clear that the linear term on the right side of (2.14) is a convolution, making its transform

$$-\frac{\omega^2}{c^2}\hat{\chi}^{(1)}(\vec{r},\omega)\hat{S}(\vec{r},\omega). \tag{2.17}$$

Subtracting this term from the left side of (2.16) yields

$$\left(\nabla^2 + \frac{\omega^2}{c^2}\left(1+\hat{\chi}(\vec{r},\omega)\right)\right)\hat{S} = (\nabla^2 + \widetilde{k}^2(\omega))\hat{S}, \tag{2.18}$$

corresponding to the linear part of the transform of (2.15), where

$$\widetilde{k}(\omega) = \frac{\omega n(\omega)}{c}, \text{ and } n(\omega) = \sqrt{1+\hat{\chi}^{(1)}(\omega)}. \tag{2.19}$$

These symbols should be familiar, as $k(\omega)$ is known as the wave number and $n(\omega)$ the *general medium index of refraction.* In the case of an instantaneous linear material response in the fiber core, the two are constants.

The last term of (2.15) is the nonlinear triple integral term. After defining

$$\hat{\chi}^{(3)}(\vec{r},u,v,\omega)=\iiint_{\Re^3}\hat{\chi}^{(3)}(\vec{r},\vec{\tau})e^{iu\tau_1}e^{iv\tau_2}e^{i\omega\tau_3}d\vec{\tau}, \tag{2.20}$$

the three-dimension Fourier transform, the nonlinear term also contains a convolution. Applying the transform will yield the transformed nonlinear component of (2.15),

$$-\frac{3\omega^2}{16\pi^2c^2}\iint_{\Re^2}\hat{\chi}^{(3)}(u,v-u,v-\omega)\hat{S}(u)\hat{S}(v-u)\hat{S}^*(v-\omega)dudv, \tag{2.21}$$

where again for simplicity the spatial dependence has been omitted. The final form of the Fourier transform of (2.15) is

$$\left(\nabla^2+\widetilde{k}^2(\omega)\right)\hat{S}=-\frac{3\omega^2}{16\pi^2c^2}\iint_{\Re^2}\hat{\chi}^{(3)}(u,v-u,\omega-v)\hat{S}(u)\hat{S}(v-u)\hat{S}^*(v-\omega)dudv. \tag{2.22}$$

Postulating that $\hat{S}$ is separable into transverse and longitudinal variables, $\hat{S}(x,y,z,\omega)=F(x,y,\omega)\hat{U}(z,\omega)e^{i\beta(\omega)z}$. Separation of variables is often a reasonable assumption when analyzing waves. Substituting, the left side of (2.22) becomes

$$\left(\nabla_T^2F\right)\hat{U}e^{i\beta(\omega)z}+\left(\hat{U}_{zz}+2i\beta(\omega)\hat{U}_z-\beta^2(\omega)\hat{U}\right)Fe^{i\beta(\omega)z}+\widetilde{k}^2(\omega)F\hat{U}e^{i\beta(\omega)z}, \tag{2.23}$$

where ∇_T^2 is the transverse Laplacian, $\nabla_T^2=\frac{\partial^2}{\partial x^2}+\frac{\partial^2}{\partial y^2}$ and the z subscript denotes a derivative. In the SVEA, since the envelope is slowly varying, $\hat{U}_{zz}$ is assumed to be small in comparison to the other terms. Dropping this term leaves

$$\left(\nabla_T^2F+\left(\widetilde{k}^2(\omega)-\beta^2(\omega)\right)F\right)\hat{U}e^{i\beta(\omega)z}+2i\beta(\omega)\hat{U}_zFe^{i\beta(\omega)z}. \tag{2.24}$$

The left–hand side resembles the standard free-space wave equation in the frequency domain. By imposing the weakly guiding conditions this term can be set equal to zero, $\nabla_T^2F+\left(\widetilde{k}^2(\omega)-\beta^2(\omega)\right)F=0$. This corresponds to choosing

β as the propagation constant of the fundamental mode and $F(x, y, \omega)$ to satisfy the index of refraction requirements at the core-cladding interface. The resulting simplification of (2.22) is

$$2i\beta(\omega)\hat{U}_z F = -\frac{3\omega^2}{16\pi^2 c^2} \iint_{\Re^2} \hat{\chi}^{(3)} F(u)F(v-u)F^*(v-\omega) \times \hat{U}(u)\hat{U}(v-u)\hat{U}^*(v-\omega)e^{i\Delta\beta(\omega)z}dudv, \tag{2.25}$$

where $\Delta\beta(\omega) = \beta(u) + \beta(v-u) - \beta(v-\omega) - \beta(\omega)$. Equation (2.25) corresponds to the general form of the slowly varying NLSE in the frequency domain.

The slowly varying NLSE (2.25) can be simplified further by removing the transverse dependence. This is done by confining (x, y) to the fiber core [10], where the nonlinear susceptibility $\chi^{(3)}$ is assumed to be independent of (x, y), and then integrating over the area of (x, y). This integration is described by

$$R_1(\omega) = \iint_{\Re^2} F(x, y, \omega)dxdy, \text{ and} \tag{2.26}$$

$$R_2(u, v, \omega) = \iint_{\Re^2} F(x, y, u)F(x, y, v)F^*(x, y, \omega)dxdy; \tag{2.27}$$

which puts equation (2.25) in the form

$$\hat{U}_z R_1(\omega) = -\frac{3\omega^2}{32i\pi^2\beta(\omega)c^2} \iint_{\Re^2} \hat{\chi}^{(3)} R_2(u, v-u, v-\omega)e^{i\Delta\beta(\omega)z}dudv. \tag{2.28}$$

Since $\beta(\omega)$ depends on the cladding and core materials index of refraction, β is bounded by $n_2^2k^2(\omega) \leq \beta^2(\omega) \leq n_1^2k^2(\omega)$. Then $n_2 \leq \frac{\beta^2(\omega)}{k^2(\omega)} \leq n_1$; despite the frequency dependence, in the weakly guided condition $n_1 \cong n_2$, $\frac{\beta^2(\omega)}{k^2(\omega)}$ is approximately a constant. In practice R_1 and R_2 are usually only weakly dependent on frequency and are generally considered constants [7]. Defining the constant $\xi = \frac{3\omega^2 R_2}{32\pi^2\beta(\omega)c^2R_1}$ yields

$$\hat{U}_z = i\xi \iint_{\Re^2} \chi^{(3)}\hat{U}(u)\hat{U}(v-u)\hat{U}^*(v-\omega)e^{i\Delta\beta(\omega)z}. \tag{2.29}$$

The nonlinear susceptibility in its simplest form would be a Dirac delta function multiplied by a constant, $\chi^{(3)}(x, y, z, t_1, t_2, t_3) = constant \bullet \delta(t_1, t_2, t_3)$. Then the transform would also be a constant and can be included by defining $\xi' = \xi\hat{\chi}^{(3)}$, resulting in

$$\hat{U}_z = i\xi' \iint_{\Re^2} \hat{U}(u)\hat{U}(v-u)\hat{U}^*(v-\omega)e^{i\Delta\beta(\omega)z}. \tag{2.30}$$

Consider the power series expansion of $\beta(\omega)$ around ω_0:

$$\beta(\omega) = \beta_0 + \beta_1(\omega - \omega_0) + \frac{\beta_2}{2}(\omega - \omega_0)^2 + \mathcal{O}(3). \tag{2.31}$$

This will allow the exponent to be simplified as

$$\begin{aligned} \Delta\beta &= \beta(u) + \beta(v-u) - \beta(v-\omega) - \beta(\omega) \\ &= \frac{\beta_2}{2}\left[(u - \omega_o^2) + (v - u - \omega_0)^2 - (v - \omega - \omega_0)^2 - (\omega - \omega_0)^2\right], \end{aligned} \tag{2.32}$$

where the higher order terms have been truncated.

Finally, define the envelope in the spectral domain as

$$\hat{A}(z, \omega - \omega_0) = \hat{U}(z, \omega)e^{i(\beta_2/2)(\omega-\omega_0)^2 z}. \tag{2.33}$$

Applying this to (2.30) gives the equation

$$\hat{A}_z(z,\omega) - i\frac{\beta_2}{2}\omega^2\hat{A}(z,\omega) = i\xi'(\omega - \omega_0)\iint_{\Re^2} \hat{A}(z,u)\hat{A}(z,v-u)\hat{A}^*(z,v-\omega)dudv, \tag{2.34}$$

where $\xi'(\omega - \omega_0)$ represents the frequency shift. The result of applying the inverse Fourier transform is the NLSE:

$$i\frac{\partial A}{\partial z} = (\beta_2/2)\frac{\partial^2 A}{\partial t^2} - \gamma|A|^2 A, \tag{2.35}$$

where the constant γ, the *Kerr* coefficient, is generally associated with the nonlinearity of the medium.

The purpose of this derivation is to both offer insight into where this equation comes from and to shed light on the approximations involved. This is the generally accepted mathematical device for the analysis of nonlinear pulse propagation in fibers. Some of the simplifications are not strictly necessary and result in additional terms, which have been omitted. For example, including the third order term β_3 from the expansion of β results in additional terms corresponding to the shock effect and the delayed Raman response [7].

The most significant term that was omitted is the term corresponding to attenuation. The total energy in the pulse is

$$E = \int_{-\infty}^{\infty} |A(z,t)|^2 dt. \tag{2.36}$$

Taking the derivative with respect to z yields

$$\frac{dE}{dz} = \int_{-\infty}^{\infty} [A(z,t)A(z,t)^*]_z dt = \int_{-\infty}^{\infty} [AA_z^* + A_z A^*] dt. \tag{2.37}$$

Then substituting the NLSE (2.35) in (2.37) and integrating by parts yields $dE/dz = 0$. This shows that conservation of energy holds [1]. In practice attenuation can be applied by considering β_2 complex, where the imaginary component represents loss. Writing the attenuation term explicitly results in a modified NLSE,

$$i\frac{\partial A}{\partial z} = (\beta_2/2)\frac{\partial^2 A}{\partial t^2} - \gamma|A|^2 A - i\alpha A, \tag{2.38}$$

where α is the attenuation coefficient of the fiber.

The model derived in the next section will require that conservation of energy hold. Loss in general is extremely small and can be compensated for through the use of optical amplifiers as demonstrated by Mollenauer et al. [11]. In general the model will still be valid, but the values of the coefficients will be modified as a result of adding amplifiers into fiber length.

2.2 The Variational Model

The variational approach employs a concept similar to the Hamiltonian used in physics. The concept is to apply the calculus of variations to associate differential equations with real-valued functions such that the extremal of the functional coincides with the solution of the differential equation. In general the functionals correspond to energy terms. In the Hamiltonian such terms would be the kinetic and potential energies. The general form of the energy function is

$$J(y) = \int_a^b L\left(x, y(x), y'(x)\right) dx, \tag{2.39}$$

where the function $L\left(x, y(x), y'(x)\right)$ is called the *Lagrangian*. The reduction to the ODE occurs by requiring the function $y(x)$ to be a minimum for the energy functional $J(y)$. This results in the ODE

$$\frac{\partial L}{\partial x} - \frac{\partial}{\partial x}\left(\frac{\partial L}{\partial y'}\right) = 0, \tag{2.40}$$

referred to as *Euler's equation*.

Anderson [12] found that there existed a Lagrangian for a system of equations equivalent to the NLSE (2.35). This required looking at the calculus of variations applied to coupled systems of partial differential equations. For two–dimensional systems, the functionals will be of the form

$$J(u, v) = \iint_{\Re^2} L(x, y, u, v, u_x, v_x, u_y, v_y) dx dy. \tag{2.41}$$

Then the equivalents to Euler's equation (2.40), of $(u(x, y), v(x, y))$ being a minimum of $J(u, v)$ are the conditions

$$\frac{\partial L}{\partial u} - \frac{\partial L_{u_x}}{\partial x} - \frac{\partial L_{u_y}}{\partial y} = 0, \text{ and} \tag{2.42}$$

$$\frac{\partial L}{\partial v} - \frac{\partial L_{v_x}}{\partial x} - \frac{\partial L_{v_y}}{\partial y} = 0, \tag{2.43}$$

where the subscripts denote derivatives. The equivalent functional for the NLSE is

$$L(u,v) = \frac{i}{2}(uv_x - vu_x) - \frac{\beta_2}{2}u_y v_y + \frac{\gamma}{2}u^2 v^2, \tag{2.44}$$

with the identification $x = z$, $y = t$, $u = A$, and $v = A^*$; then

$$L = \frac{i}{2}(AA_z^* - A^* A_z) - \frac{\beta_2}{2}A_t A_t^* + \frac{\gamma}{2}A^2 A^{*^2}. \tag{2.45}$$

Applying the conditions for a minimum: (2.42) corresponds to the NLSE (2.35) and (2.43) corresponds to the complex conjugate of the NLSE.

The variational approach uses the Lagrangian found by Anderson [12] and combines it with the Ritz procedure [13]. The Ritz procedure reduces the infinite space of the forms of the envelope $A(z,t)$ to a space of *finitely-parameterized* pulse shapes. Then minimizing the functional (2.45) over this restricted class will result in differential equations that describe the evolution of the pulse parameters.

A commonly used envelope form is the class of parameterized Gaussians. There are several reasons to choose this class over other pulses. It is a realistic shape, and it is often used in experiments [7]. Also, the Gaussian has been shown to retain its shape for both numerical simulation and experimentation in realistic nonlinear fibers under normal dispersion and low nonlinearity conditions. Such a class can be applied to a length of the fiber without concern for the pulse shape leaving the chosen class. Since in the linear limit the Gaussian pulse will reduce exactly to the NLSE (2.35), Gaussian pulses of the form

$$A(z,t) = M(z)exp\left[-t^2\left(\frac{1}{2a(z)^2} - ib(z)\right)\right], \tag{2.46}$$

are a better choice than other soliton solutions such as hyperbolic secant shaped pulses.

Inserting the ansatz (2.46) into the Lagrangian $L(A, A^*)$ (2.45), and

integrating over time leaves only the space integral

$$J(A, A^*) = \int_{\Re} \langle L \rangle dz, \tag{2.47}$$

where

$$\langle L \rangle = \frac{\sqrt{\pi}}{2} \left[ia \left(M \frac{dM^*}{dz} - M^* \frac{dM}{dz} \right) + |M|^2 a^3 \frac{db}{dz} - a^3 |M|^2 \frac{\beta_2}{2} \left(4b^2 + \frac{1}{a^4} \right) - \frac{1}{\sqrt{2}} \gamma a |M|^4 \right]. \tag{2.48}$$

Applying the calculus of variations to minimize the functional (2.47) results in four equations derived in minimizing with respect to the parameters describing the pulse, namely $M(z)$, $M^*(z)$, $a(z)$, and $b(z)$. The coupled ODEs are

$$\frac{\delta \langle L \rangle}{\delta M} = 0 \Rightarrow \frac{d}{dz}(iaM^*) = -ia\frac{dM^*}{dz} + M^* a^3 \frac{db}{dz} - a^3 M^* \frac{\beta_2}{2} \left(4b^2 + \frac{1}{a^4} \right) - \sqrt{2}\gamma a |M|^2 M, \tag{2.49}$$

$$\frac{\delta \langle L \rangle}{\delta M^*} = 0 \Rightarrow \frac{d}{dz}(iaM) = -ia\frac{dM}{dz} + M a^3 \frac{db}{dz} - a^3 M \frac{\beta_2}{2} \left(4b^2 + \frac{1}{a^4} \right) - \sqrt{2}\gamma a |M|^2 M, \tag{2.50}$$

$$\frac{\delta \langle L \rangle}{\delta a} = 0 \Rightarrow i \left(M \frac{dM^*}{dz} - M^* \frac{dM}{dz} \right) + 3|M|^2 a^2 \frac{db}{dz} - 6\beta_2 a^2 b^2 |M|^2 + \frac{\beta_2}{2} \frac{|M|^2}{a^2} - \frac{1}{\sqrt{2}} \gamma |M|^4 = 0, \text{ and} \tag{2.51}$$

$$\frac{\delta \langle L \rangle}{\delta b} = 0 \Rightarrow \frac{d}{dz}(a^3 |M|^2) = -4\beta_2 b a^3 |M|^2. \tag{2.52}$$

Subtracting (2.49)$\times M$ from (2.50)$\times M^*$ results in

$$\frac{d}{dz}(a|M|^2) = 0, \tag{2.53}$$

while adding (2.49)$\times M$ to (2.50)$\times M^*$ results in

$$i \left(M^* \frac{dM}{dz} - M \frac{dM^*}{dz} \right) = |M|^2 \left[a^2 \frac{db}{dz} - a^2 \frac{\beta_2}{2} \left(4b^2 + \frac{1}{a^4} \right) - \sqrt{2}\gamma |M|^2 \right]. \tag{2.54}$$

The first equation (2.53) is equivalent to the conversation of energy result already obtained from the NLSE, which can be stated as

$$a(z)|M(z)|^2 = \text{ constant } = a_0|M_0|^2 = a_0P_0 = E_0, \tag{2.55}$$

where P_0 is the peak power and E_0 is a multiple of the pulse energy. Applying this result to (2.52) yields

$$\frac{da}{dz} = -2\beta_2 a(z)b(z). \tag{2.56}$$

Using the like terms (2.51) and (2.54), the result can be combined and simplified to yield

$$a\frac{db}{dz} - 2\beta_2 ab^2 + \frac{\beta}{2a^3} + \frac{\gamma}{2\sqrt{2}}\frac{|M|^2}{a}. \tag{2.57}$$

Replacing the constant given by (2.55) with $|M|^2$,

$$|M|^2 = \frac{a(z)|M(z)|^2}{a(z)} = \frac{a_0P_0}{a(z)} \tag{2.58}$$

allows equation (2.57) to simplify:

$$a\frac{db}{dz} = 2\beta_2 ab^2 - \frac{\beta}{2a^3} - \frac{\gamma a_0P_0}{2\sqrt{2}a^2}. \tag{2.59}$$

After differentiating (2.56),

$$\frac{d^2a}{dz^2} = -2\beta_2\left(a\frac{db}{dz} + b\frac{da}{dz}\right); \tag{2.60}$$

the result can be written as

$$a\frac{db}{dz} = -b\frac{da}{dz} - \frac{1}{2\beta_2}\frac{d^2a}{dz^2}. \tag{2.61}$$

Equating (2.59) and (2.61) yields the second order ODE

$$\frac{d^2a}{dz^2} = \frac{\beta_2^2}{a(z)^3} + \frac{\beta_2 a_0\gamma P_0}{\sqrt{2}a(z)^2}. \tag{2.62}$$

In order to simplify the number of variables, the constant $\kappa = \frac{\gamma P_0}{\sqrt{2}}$ will be used, resulting in a second order differential equation

$$\frac{d^2a}{dz^2} = \frac{\beta_2^2}{a(z)^3} + \frac{\beta_2 a_0 \kappa}{a(z)^2}. \tag{2.63}$$

The variational model has been demonstrated to yield results that closely correlate to simulations of the NLSE [1]. This model will be used to develop control laws that produce solitons. The input to this system, the dispersion coefficient β_2, enters the system in both a squared and linear manner, making this system radically different from classical control systems.

CHAPTER 3

TUNABLE DISPERSION MATERIALS

In this chapter tunable dispersion technology is examined. This encompasses a large field of devices including fiber gratings, thin film etalons, and bulk optics. Each has both positive and negative features, making it unclear which method will achieve the theoretical fiber we visualize; therefore, this chapter will give a brief overview of each area.

Using fiber gratings to create tunable dispersion is usually accomplished by incorporating a small fiber grating into a long length of the fiber. The grating adds additional dispersion to the system. It is normally used as a compensator because it counteracts the dispersion and nonlinear effects that result from propagating a pulse down a long section of fiber. The basic principle behind almost all fiber grating dispersion compensators is Bragg reflection.

The dispersion is tuned by modifying the grating spacing through a variety of methods. To date, thermal methods have been the most successful commercially because of their high reliability, low polarized mode dispersion (PMD) and lack of moving parts [6]. The primary mechanism is the application of heat or cooling to the grating. The latest technology embeds heating elements in a thin film along the outside of the fiber at the site of the grating [14]. Then a current is applied, resulting in a I^2R heating. One of the primary limitations of such gratings is the slow response time.

An alternative to thermal gratings is strain gratings. These grating are tuned by applying strain, usually accomplished through piezo-electric materials. The advantage of strain gratings is that response times may be more than one hundred times faster than those of thermally tuned gratings [6]. Also, straining

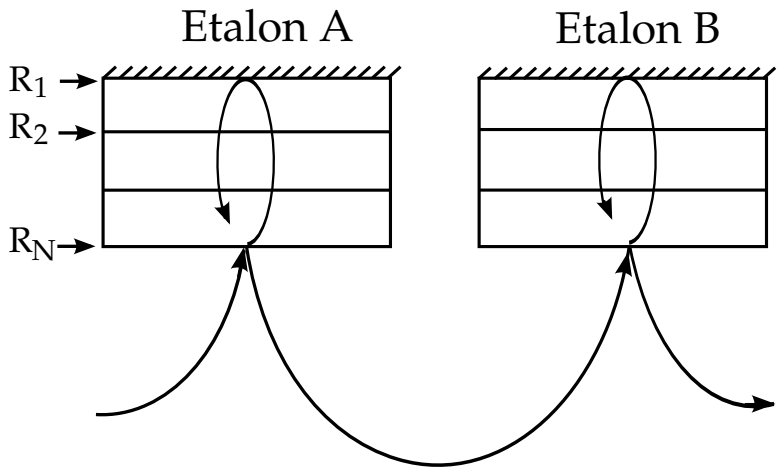

Figure 3.1: Schematic of multi-cavity etalon tunable dispersion compensator. The etalons have a reflective interface between each cavity with only R being close to 100% reflective.

can in principle change a Bragg resonance by more than ten times the maximum thermal change, which results in larger tuning ranges; however, this is at the expense of long-term reliability. Strain gratings are also limited in applicability due to excess PMD.

While it is more common to introduce small lengths of fiber grating as a compensator, gratings over large area of the fiber have been demonstrated in telecom systems [15]. This provides almost arbitrary dispersion and dispersion slope over large bandwidths. The problem from a feedback standpoint is that such fibers cannot be easily tuned, since their length precludes the strain and thermal tuning possible with shorter gratings.

The etalon is a tunable dispersion device whose basic operation is resonance-based. As shown in Figure 3.1, a cavity consists of N reflective interfaces with varying percentages of reflectivity [16]. The arrows represent the light path. The cavities and interfaces are built so as to generate the desired dispersion. Each cavity is constructed so that a resonance will be experienced at a center frequency. Modifying the number of cavities, spacing, and strain of the material will affect where the resonance occurs and thus the amount of group delay experienced by a light wave. Multiple etalons can be spread along the

fiber so that the dispersion map can be tuned appropriately. Tunability is achieved through strain on one or more of the cavities of etalon. This strain can be applied by external heating or by applying a voltage across the material. Voltage straining necessitates an analog range in order to achieve the desired strain. To fine tune the dispersion along a fiber, multiple devices must be used. A drawback of tunable resonant dispersion compensators is that typically they have large loss due to coupling to bulk optics or planar waveguides. Typical insertion loss is 4-6 dB as compared to 2-3 dB for tunable fiber gratings [6].

Bulk optic techniques use a dispersion compensation mechanism that is directly embedded throughout the length of the fiber. This is in contrast to methods previously discussed, which require the addition of devices spaced along the length of fiber, and which incur insertion loss. Some of the most promising work is the development of tunable photonic band gap fibers. Photonic band gap fibers use alternating layers of dielectric material, which give rise to two-dimensional Bragg scattering, forming a photonic band gap in the cladding. Frequencies which lie within the photonic band gap are not allowed to propagate within the cladding and are localized in the low index fiber core. One design uses a solid silica core surrounded by a triangular lattice of air holes. The holes are filled with a high index liquid, $n_{589nm} = 1.80$ [17]. The index of the material within the holes is adjusted continuously by varying the temperature. This leads to changes in the photonic band gap spectra from the spacing and widths of the band gaps.

Varying the geometry of the holes and using different liquids can result in a wide range of possible dispersion ranges. In Figure 3.2, which is taken from [18], two liquids are used in a hexagonal pattern to generate very high negative chromatic dispersion values, $D = -19\,000$ ps/(nm·km). These fibers are limited in that dispersion is tuned thermally and the response is slow. Also, the high dispersion values available do not necessarily coincide with large ranges. There may be only a small range of dispersion values possible, but they may be at extreme values. Despite these issues, the photonic band gap fiber's low loss and

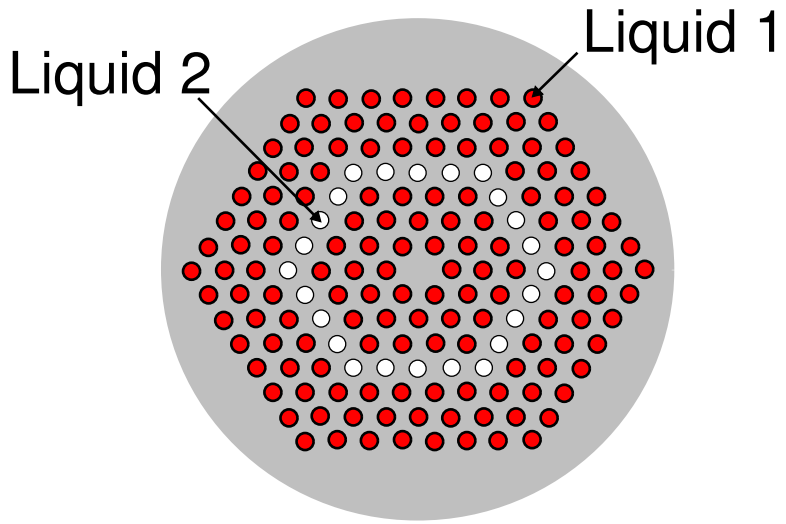

Figure 3.2: Cross-sectional view of the dual-core liquid-filled photonic core fiber for dispersion compensation. Very large negative dispersion can be generated through the choice of geometry and liquids.

the continuous control along the fiber make it a strong contender for matching the properties we desire for feedback control.

While tunable dispersion fibers have been developed, they are still severely limited in their ability to implement standard control algorithms. The physical object considered in this thesis does not yet exist, but the breakthroughs in tunable dispersion material should be treated as opportunities to explore possible uses for such a material. Our vision is to incorporate it into a tunable dispersion fiber that could be controlled by actuators that would control the dispersion over an infinitely small length dl, over the total fiber length L. These actuators will take some kind of signal and convert it into the appropriate dispersion within the fiber. These sections can be made as small as desired so that the dispersion can be changed continuously along the fiber. Coupling between different sections would allow the interfaces between section lengths to be controlled. The theorized result is a fiber in which the dispersion map can be controlled continuously and actuators can respond quickly enough to render the response time approximately instantaneous.

CHAPTER 4

INTRODUCTION TO THE NORMAL FORM

Before applying control to the model developed in Chapter 2, it is important to understand normal form theory. The normal form provides a tool for finding a coordinate system in which the dynamical system takes the "simplest" form. The coordinate transformation will be derived as well as the resulting "simplest" dynamical system. The method is local in the sense that the transformation and resulting system are valid only in a neighborhood of a known solution. In addition, the linear part of the system will determine the structure of the resultant form; the higher order dynamics will only affect the parameter values of the transformed system.

This chapter will present an introduction to the normal form as in [19]. The first requirement is that the transform be local in terms of a known solution. In this case a fixed point will be used. By definition, at a fixed point the vector field is zero and thus the solution at this point is known for all time. Consider the system

$$\dot{w} = W(w),\ w \in \mathbb{R}^n, \tag{4.1}$$

with a fixed point at $w = w_0$. Performing the coordinate shift

$$v = w - w_0,\ v \in \mathbb{R}^n, \tag{4.2}$$

shifts the fixed point to the origin and transforms (4.1) into

$$\dot{v} = W(v + w_0) \equiv H(v). \tag{4.3}$$

The next step is to break the system into linear and nonlinear parts by writing (4.3) as

$$\dot{v} = \nabla H(0)v + \bar{H}(v), \tag{4.4}$$

where $\bar{H}(v) = H(v) - \nabla H(0)v$. Notice that $\bar{H}$ now contains only dynamics of order two and above. Now the linear part should be placed in real Jordan canonical form via the transformation

$$v = Tx, \tag{4.5}$$

which puts (4.4) into the form

$$\dot{x} = T^{-1}\nabla H(0)Tx + T^{-1}\bar{H}(Tx) = Jx + F(x), \tag{4.6}$$

where J and F are defined as

$$J \equiv T^{-1}\nabla H(0)T, \text{ and} \tag{4.7}$$

$$F(x) \equiv T^{-1}\bar{H}(Tx). \tag{4.8}$$

The fixed point has been moved to the origin and the system has been put in the real Jordan form. Now the nonlinear part must be simplified. The Taylor expansion will be applied to $F(x)$ which results in (4.6) becoming

$$\dot{x} = Jx + F_2(x) + F_3(x) + ... + F_{r-1}(x) + \mathcal{O}(|x|^r), \tag{4.9}$$

where $F_i(x)$ represents the order i terms. We introduce the close-to-identity coordinate transformation $x = \Gamma(y)$, given by

$$x = y + \Gamma_2(y) + \Gamma_3(y) + ... + \Gamma_{r-1}(y) + \mathcal{O}(|y|^r). \tag{4.10}$$

The sequence of coordinate transformations will be considered at each order.

4.1 Second Order Terms

Only the second order terms of the transform will be considered for the first coordinate transformation, thus

$$x = y + \Gamma_2(y). \tag{4.11}$$

Following [19], we substitute (4.11) into (4.9) and obtain

$$\begin{aligned}\dot{x} = (I + \nabla\Gamma_2(y))\dot{y} = Jy + J\Gamma_2(y) + F_2(y + \Gamma_2(y)) \\ + F_3(y + \Gamma_2(y)) + ... + F_{r-1}(y + \Gamma_2(y)) + \mathcal{O}(|y|^r).\end{aligned} \tag{4.12}$$

Each term $F_k(y + \Gamma_2(y))$, for $2 \leq k \leq r - 1$, can be written as

$$F_k(y) + \mathcal{O}(|y|^{k+1}) + ... + \mathcal{O}(|y|^{2k}). \tag{4.13}$$

Then (4.12) becomes

$$\begin{aligned}(I + \nabla\Gamma_2(y))\dot{y} = Jy + J\Gamma_2(y) + F_2(y) + \widetilde{F}_3(y) \\ + ... + \widetilde{F}_{r-1}(y) + \mathcal{O}(|y|^r),\end{aligned} \tag{4.14}$$

where $\widetilde{F}_k(y)$ contains all terms of order k resulting from applying expansion (4.13) to all the $F_j(y)$ terms with $j \leq k$.

For y sufficiently small, $(I + \nabla\Gamma_2(y))^{-1}$ will exist, and

$$(I + \nabla\Gamma_2(y))^{-1} = I - \nabla\Gamma_2(y) + \mathcal{O}(|y|^2). \tag{4.15}$$

Applying (4.15) to (4.14) gives

$$\begin{aligned}\dot{y} = Jy + J\Gamma_2(y) - \nabla\Gamma_2(y)Jy + F_2(y) + \widetilde{F}_3(y) \\ + ... + \widetilde{F}_{r-1}(y) + \mathcal{O}(|y|^r).\end{aligned} \tag{4.16}$$

The goal is generally to put the dynamical system $\dot{y}$ in the simplest form possible, so if Γ_2 can be chosen such that

$$\nabla\Gamma_2(y)Jy - J\Gamma_2(y) = F_2(y), \tag{4.17}$$

then the second order terms in $\dot{y}$ will sum to zero.

Consider (4.17) as a linear equation with Γ_2 unknown. Then consider $\Gamma_2(y)$ as an element of P_2, where P_k is the space of all homogeneous polynomials of degree k. The map

$$\Gamma_2(y) \longmapsto \nabla\Gamma_2(y)Jy - J\Gamma_2(y) \tag{4.18}$$

is a linear map from P_2 into P_2. It is not surprising that the mapping

$$\Gamma_k(y) \longmapsto \nabla\Gamma_k(y)Jy - J\Gamma_k(y) \tag{4.19}$$

will also be a linear map from P_k into P_k for every order k. Relating to traditional terminology, this map is denoted as

$$L_J^{(k)}(\Gamma_k(y)) \equiv [\Gamma_k(y), Jy] = (\nabla\Gamma_k(y)Jy - J\Gamma_k(y)), \tag{4.20}$$

where $[\cdot,\cdot]$ denotes the Lie bracket operation.

Returning to the second order term (4.17), this equation,

$$-L_J^{(2)}(\Gamma_2) = F_2(y), \tag{4.21}$$

is equivalent to solving a linear system of the form $Ax = b$ with $A = -L_J^{(2)}(\cdot)$, $x = \Gamma_k(y)$, and $b = F_2(y)$. If $F_2(y)$ is in the range of $L_J^{(2)}(\cdot)$ then all second order terms can be eliminated. This is computed by applying a finite dimensional version of the *Fredholm alternative*:

$$b \in Range\, A \Leftrightarrow b \in (Ker\, A^*)^{\perp}. \tag{4.22}$$

Second order terms can be simplified by the choice of Γ_2. The terms that are left will be denoted by

$$F_2^r(y) \in \left(KerL_J^{(2)}(\cdot)\right)^{\perp}. \tag{4.23}$$

4.2 Higher Order Terms

Now consider the third order terms through the map

$$y \longmapsto y + \Gamma_3(y). \tag{4.24}$$

After applying the same sequence of algebraic manipulations the result will be

$$\begin{aligned} \dot{y} = Jy + F_2^r(y) + J\Gamma_3(y) - \nabla\Gamma_3(y)Jy + \widetilde{F}_3(y) + \widetilde{F}_4(y) \\ + ... + \widetilde{F}_{r-1}(y) + \mathcal{O}(|y|^r). \end{aligned} \tag{4.25}$$

This is identical to (4.17), with the remaining second order simplification and the second order terms replaced by third order terms. The simplification of the third order terms is identical to the second order simplification, as it involves solving

$$\nabla\Gamma_3(y)Jy - J\Gamma_3(y) = \widetilde{F}_3(y). \tag{4.26}$$

The remaining third order term will then be

$$F_3^r(y) \in \left(KerL_J^{(3)}(\cdot)\right)^{\perp}. \tag{4.27}$$

This procedure can be followed to order $r-1$ with a resulting form of

$$\dot{y} = Jy + F_2^r(y) + \ldots + F_{r-1}^r(y) + \mathcal{O}(|y|^r), \tag{4.28}$$

where the resonant terms denoted by the superscript are

$$F_k^r(y) \in \left(KerL_J^k(\cdot)\right)^{\perp}. \tag{4.29}$$

Note that the resonant terms are all determined through the Jacobian J, the linear part. It is for this reason that any system with the same eigenvalues will locally behave similarly.

CHAPTER 5

THE HOPF BIFURCATION

According to normal form theory, the local dynamics of a system will be determined by the linear part of a system through its eigenvalues. In this chapter we will review the normal form of the Poincaré-Andronov-Hopf bifurcation, often referred to simply as the Hopf bifurcation, and examine its properties.

5.1 Hopf Normal Form

In order for a system to be transformed into a Hopf normal form, it must have two purely imaginary eigenvalues. Since the normal form for a Hopf bifurcation is generally described up to third order, terms up to third order will be considered in the derivation.

Consider the system

$$\dot{x} = f(x, \mu), \ x \in \mathbb{R}^2, \tag{5.1}$$

where μ is a parameterization and $\nabla_x F(0,0)$ has two purely imaginary eigenvalues $\lambda(0) = \pm i\omega(0)$. The linear part of the system can be transformed into real Jordan form such that $\nabla_x f(0,\mu)$ is of the form

$$\nabla_x f(0,\mu) = \begin{pmatrix} \text{Re } \lambda(\mu) & -\text{Im } \lambda(\mu) \\ \text{Im } \lambda(\mu) & \text{Re } \lambda(\mu) \end{pmatrix} \tag{5.2}$$

for μ sufficiently small, in the neighborhood of zero.

The next few steps are not strictly necessary; however, they add perspective because the two eigenvalues will be complex conjugates. For this reason the

system can be described by a one-dimensional dynamical system and its complex conjugate, so solving one will also solve the conjugate.

Denoting

$$\text{Re } \lambda(\mu) = |\lambda(\mu)| \cos(2\pi\theta(\mu)) \text{ and} \tag{5.3}$$

$$\text{Im } \lambda(\mu) = |\lambda(\mu)| \sin(2\pi\theta(\mu)) \tag{5.4}$$

allows (5.2) to be written as

$$\nabla_x f(0,\mu) = |\lambda(\mu)| \begin{pmatrix} \cos 2\pi\theta(\mu) & -\sin 2\pi\theta(\mu) \\ \sin 2\pi\theta(\mu) & \cos 2\pi\theta(\mu) \end{pmatrix}. \tag{5.5}$$

The system (5.1) can then be written in the form

$$\begin{pmatrix} \dot{x}_1 \\ \dot{x}_2 \end{pmatrix} = |\lambda(\mu)| \begin{pmatrix} \cos 2\pi\theta(\mu) & -\sin 2\pi\theta(\mu) \\ \sin 2\pi\theta(\mu) & \cos 2\pi\theta(\mu) \end{pmatrix} \begin{pmatrix} x \\ y \end{pmatrix} + \begin{pmatrix} f_1(x_1, x_2, \mu) \\ f_2(x_1, x_2, \mu) \end{pmatrix}, \tag{5.6}$$

where f_1 and f_2 are nonlinear in x and represent the higher order terms. The system can be put in the form of a complex conjugate pair by making the linear transformation

$$\begin{pmatrix} z \\ \bar{z} \end{pmatrix} = \begin{pmatrix} 1 & i \\ 1 & -i \end{pmatrix} \begin{pmatrix} y \\ y \end{pmatrix}; \qquad \begin{pmatrix} x_1 \\ x_2 \end{pmatrix} = \frac{1}{2} \begin{pmatrix} 1 & 1 \\ -i & i \end{pmatrix} \begin{pmatrix} z \\ \bar{z} \end{pmatrix}, \tag{5.7}$$

resulting in the system

$$\begin{pmatrix} \dot{z} \\ \dot{\bar{z}} \end{pmatrix} = |\lambda| \begin{pmatrix} e^{i2\pi\theta} & 0 \\ 0 & e^{-i2\pi\theta} \end{pmatrix} \begin{pmatrix} z \\ \bar{z} \end{pmatrix} + \begin{pmatrix} F^1(z, \bar{z}, \mu) \\ F^2(z, \bar{z}, \mu) \end{pmatrix}, \tag{5.8}$$

where

$$F^1(z,\bar{z},\mu) = f_1(x_1(z,\bar{z}), x_2(z,\bar{z}), \mu) + i f_2(x_1(z,\bar{z}), x_2(z,\bar{z}), \mu),$$
$$F^2(z,\bar{z},\mu) = f_1(x_1(z,\bar{z}), x_2(z,\bar{z}), \mu) - i f_2(x_1(z,\bar{z}), x_2(z,\bar{z}), \mu).$$

Since $\dot{\bar{z}}$ is simply the complex conjugate of $\dot{z}$, transforming

$$\dot{z} = |\lambda| e^{i2\pi\theta} z + F_1(z, \bar{z}, \mu) \tag{5.9}$$

into normal form will also transform $\bar{z}$ into normal form.

Expanding (5.9) in the Taylor series yields

$$\dot{z} = |\lambda| e^{i2\pi\theta} z + F_2 + F_3 + \ldots + F_{r-1} + \mathcal{O}(|z|^r, |\bar{z}|^r), \tag{5.10}$$

where the F_j are polynomials in z and $\bar{z}$ of order j with coefficients depending on μ. Applying the linear map

$$z \longmapsto z + h_2(z, \bar{z}), \tag{5.11}$$

where the μ dependence exists but is not displayed, (5.10) becomes

$$\dot{z}\left(1 + \frac{\partial h_2}{\partial z}\right) + \frac{\partial h_2}{\partial \bar{z}}\dot{\bar{z}} = \lambda z + \lambda h_2 + F_2(z, \bar{z}) + \mathcal{O}(3) \tag{5.12}$$

which will describe the dynamics of $\dot{z}$ by

$$\dot{z} = \left(1 + \frac{\partial h_2}{\partial z}\right)^{-1} \left[\lambda z - \frac{\partial h_2}{\partial \bar{z}}\dot{\bar{z}} + \lambda h_2 + F_2(z, \bar{z}) + \mathcal{O}(3)\right]. \tag{5.13}$$

Since locally z and $\bar{z}$ can be taken sufficiently small, the inverse

$$\left(1 + \frac{\partial h_2}{\partial z}\right)^{-1} = 1 - \frac{\partial h_2}{\partial z} + \mathcal{O}(2) \tag{5.14}$$

will exist; therefore, up to order two,

$$\dot{z} = \lambda z - \lambda \frac{\partial h_2}{\partial z} z - \bar{\lambda} \frac{\partial h_2}{\partial \bar{z}} \bar{z} + \lambda h_2 + F_2 + \mathcal{O}(3), \tag{5.15}$$

$$\dot{\bar{z}} = \bar{\lambda}\bar{z} + \bar{F}_2 + \mathcal{O}(3). \tag{5.16}$$

Then the second order terms can be eliminated if an h_2 can be found such that

$$\lambda h_2 - \left(\lambda \frac{\partial h_2}{\partial z} z + \bar{\lambda} \frac{\partial h_2}{\partial \bar{z}} \bar{z}\right) = F_2. \tag{5.17}$$

This is equivalent to (4.17), so the map

$$h_2 \longmapsto \lambda h_2 - \left[\lambda \frac{\partial h_2}{\partial z} z + \bar{\lambda} \frac{\partial h_2}{\partial \bar{z}} \bar{z}\right] \tag{5.18}$$

is a linear map in the space of polynomials of degree two in z and $\bar{z}$ into itself; denote this space P_2. To determine if the second order terms can be eliminated, F_2 must be an element of this vector space. This can be determined by computing the action of the linear map on a basis of P_2.

P_2 can be described by the basis

$$P_2 = \text{span } \{z^2, z\bar{z}, \bar{z}^2\}. \tag{5.19}$$

Applying the linear map (5.18) to each of the basis elements results in

$$\lambda z^2 - \left[\lambda \left(\frac{\partial}{\partial z} z^2\right) z + \bar{\lambda} \left(\frac{\partial}{\partial \bar{z}} z^2\right) \bar{z}\right] = -\lambda z^2, \tag{5.20}$$

$$\lambda z\bar{z} - \left[\lambda \left(\frac{\partial}{\partial z} z\bar{z}\right) z + \bar{\lambda} \left(\frac{\partial}{\partial \bar{z}} z\bar{z}\right) \bar{z}\right] = -\bar{\lambda} z\bar{z}, \tag{5.21}$$

$$\lambda \bar{z}^2 - \left[\lambda \left(\frac{\partial}{\partial z} \bar{z}^2\right) z + \bar{\lambda} \left(\frac{\partial}{\partial \bar{z}} \bar{z}^2\right) \bar{z}\right] = (\lambda - 2\bar{\lambda}) \bar{z}^2. \tag{5.22}$$

The matrix representation of the map (5.18) on this basis is

$$\begin{pmatrix} -\lambda(\mu) & 0 & 0 \\ 0 & -\bar{\lambda}(\mu) & 0 \\ 0 & 0 & \lambda(\mu) - 2\bar{\lambda}(\mu) \end{pmatrix}. \tag{5.23}$$

If this matrix is full rank then F_2 must be in the vector space of the linear map and thus an h_2 can be found and all second order terms eliminated. At $\mu = 0$, $\lambda(0) = -\bar{\lambda}(0) \neq 0$; therefore, for μ sufficiently small $\lambda(\mu) \neq 0$ and

$\lambda(\mu) - 2\bar{\lambda}(\mu) \neq 0$. This means that the matrix is full rank and all second order terms can be eliminated from (5.15).

After the elimination of the second order terms,

$$\dot{z} = \lambda z + F_3 + \mathcal{O}(4). \tag{5.24}$$

Now applying the linear map for the third order coordinate transform,

$$z \longmapsto z + h_3(z, \bar{z}) \tag{5.25}$$

yields

$$\begin{aligned} \dot{z} &= \left(1 + \frac{\partial h_3}{\partial z}\right)^{-1} \left[\lambda z - \frac{\partial h_3}{\partial \bar{z}}\dot{\bar{z}} + \lambda h_3 + F_3(z, \bar{z}) + \mathcal{O}(3)\right] \\ &= \lambda z - \lambda \frac{\partial h_3}{\partial z} z - \bar{\lambda}\frac{\partial h_3}{\partial \bar{z}}\bar{z} + \lambda h_3 + F_3 + \mathcal{O}(4). \end{aligned} \tag{5.26}$$

As before, the third order terms can be eliminated if

$$\lambda h_3 - \lambda \frac{\partial h_3}{\partial z} z + \bar{\lambda}\frac{\partial h_3}{\partial \bar{z}}\bar{z} = F_3 \tag{5.27}$$

can be solved. The action of the map

$$h_3 \longmapsto \lambda h_3 - \left(\lambda \frac{\partial h_3}{\partial z} z + \bar{\lambda}\frac{\partial h_3}{\partial \bar{z}}\bar{z}\right) \tag{5.28}$$

maps third order polynomials in z and $\bar{z}$ into itself (P_3).

The basis elements for P_3 are

$$P_3 = \text{span } \{z^3, z^2\bar{z}, z\bar{z}^2\bar{z}^3\}. \tag{5.29}$$

Applying the linear map (5.28) to each of the basis elements results in

$$\lambda z^3 - \left[\lambda\left(\frac{\partial}{\partial z}z^3\right)z + \bar{\lambda}\left(\frac{\partial}{\partial \bar{z}}z^3\right)\bar{z}\right] = -2\lambda z^3, \tag{5.30}$$

$$\lambda z^2\bar{z} - \left[\lambda\left(\frac{\partial}{\partial z}z^2\bar{z}\right)z + \bar{\lambda}\left(\frac{\partial}{\partial \bar{z}}z^2\bar{z}\right)\bar{z}\right] = -(\lambda+\bar{\lambda})z^2\bar{z}, \tag{5.31}$$

$$\lambda z\bar{z}^2 - \left[\lambda\left(\frac{\partial}{\partial z}z\bar{z}^2\right)z + \bar{\lambda}\left(\frac{\partial}{\partial \bar{z}}z\bar{z}^2\right)\bar{z}\right] = -2\bar{\lambda}z\bar{z}^2, \tag{5.32}$$

$$\lambda\bar{z}^3 - \left[\lambda\left(\frac{\partial}{\partial z}\bar{z}^3\right)z + \bar{\lambda}\left(\frac{\partial}{\partial \bar{z}}\bar{z}^3\right)\bar{z}\right] = (\lambda-3\bar{\lambda})\bar{z}^3. \tag{5.33}$$

The matrix representation of the map (5.28) on this basis is

$$\begin{pmatrix} -2\lambda(\mu) & 0 & 0 & 0 \\ 0 & -\left(\lambda(\mu)+\bar{\lambda}(\mu)\right) & 0 & 0 \\ 0 & 0 & -2\bar{\lambda}(\mu) & 0 \\ 0 & 0 & 0 & \lambda(\mu)-3\bar{\lambda}(\mu) \end{pmatrix}. \tag{5.34}$$

At $\mu = 0$, the term $\lambda(\mu) + \bar{\lambda}(\mu) = 0$ while none of the other terms of the matrix are identically zero. The matrix is then rank three. So for μ sufficiently small, the third order terms not of the form $z^2\bar{z}$ can be eliminated. Then the normal form up to third order is

$$\dot{z} = \lambda z + e(\mu)z^2\bar{z} + \mathcal{O}(4), \tag{5.35}$$

where $e(\mu)$ is a coefficient dependent on μ, which will be determined by the specific form of F_3.

This process can be repeated through order n. At each order the simplification will depend on whether

$$\lambda h - \left(\lambda z\frac{\partial h}{\partial z} + \bar{\lambda}\bar{z}\frac{\partial h}{\partial \bar{z}}\right) = 0 \tag{5.36}$$

for some $h = z^n\bar{z}^m$, where $m+n$ is the order of the term to be simplified. This

will cause (5.36) to become

$$\lambda z^n \bar{z}^m - (n\lambda z^n \bar{z}^m + m\bar{\lambda} z^n \bar{z}^m) = 0, \tag{5.37}$$

$$(\lambda - n\lambda - m\bar{\lambda}) z^n \bar{z}^m = 0. \tag{5.38}$$

At $\mu = 0$, $\lambda(0) = -\bar{\lambda}(0)$, which implies that if

$$1 + m - n = 0 \tag{5.39}$$

the order $m + n$ cannot be eliminated. This will never occur if m and n are even numbers; thus, all even-order terms can be eliminated and the normal form is

$$\begin{aligned} \dot{z} &= \lambda z + e(\mu) z^2 \bar{z} + \mathcal{O}(5) \\ \dot{\bar{z}} &= \bar{\lambda} \bar{z} + \bar{e}(\mu) z \bar{z}^2 + \mathcal{O}(5) \end{aligned} \tag{5.40}$$

in the neighborhood of $\mu = 0$. This can be transformed back into Cartesian coordinates by letting $\lambda(\mu) = \alpha(\mu) + i\omega(\mu)$, and $e(\mu) = j(\mu) + ik(\mu)$. Then

$$\begin{aligned} \dot{x}_1 &= \alpha x_1 - \omega x_2 + (j x_1 - k x_2)(x_1^2 + x_2^2) + \mathcal{O}(5), \\ \dot{x}_2 &= \omega x_1 + \alpha x_2 + (k x_1 + j x_2)(x_1^2 + x_2^2) + \mathcal{O}(5). \end{aligned} \tag{5.41}$$

The transformation to normal form could have been carried out completely in Cartesian coordinates, but both states would have to be considered, making the computation more time consuming. The Hopf normal form is expressed in polar coordinates as

$$\dot{r} = \alpha r + j r^3 + \mathcal{O}(r^5), \tag{5.42}$$

$$\dot{\theta} = \omega + k r^2 + \mathcal{O}(r^4). \tag{5.43}$$

Given a real system the coefficients α, ω, j, k can all be determined through the normal form method. The transformation that puts the system into the normal

form will also be computed in the process.

5.2 Dynamics of the Hopf Bifurcation

As the Hopf normal form is associated with systems with an imaginary pole pair crossing the imaginary axis, it has been the focus of much study. It is important to understand the dynamics so as to understand the local dynamics of many other similar systems. In the previous section the normal form in polar coordinates was found to be

$$\begin{aligned} \dot{r} &= \alpha(\mu)r + j(\mu)r^3 + \mathcal{O}(r^5), \\ \dot{\theta} &= \omega(\mu) + k(\mu)r^2 + \mathcal{O}(r^4). \end{aligned} \tag{5.44}$$

Near the region of interest, at $\mu = 0$ the dynamics can be Taylor expanded causing (5.44) to become

$$\begin{aligned} \dot{r} &= \alpha_\mu(0)\mu r + j(0)r^3 + \mathcal{O}(\mu^2 r, \mu r^3, r^5), \\ \dot{\theta} &= \omega(0) + \omega_\mu(0)\mu + k(0)r^2 + \mathcal{O}(\mu^2, \mu r^2, r^4). \end{aligned} \tag{5.45}$$

Recall that $\alpha(0) = 0$, which is why that term has been dropped from (5.45). The subscript μ denotes a differentiation with respect to μ.

Truncating the higher order terms and defining $\alpha_\mu(0) \equiv d$, $j(0) \equiv j_0$, $\omega(0) \equiv \omega_0$, $\omega_\mu(0) \equiv c$, $k(0) \equiv k_0$ causes (5.45) to become

$$\begin{aligned} \dot{r} &= d\mu r + j_0 r^3, \\ \dot{\theta} &= \omega_0 + c\mu + k_0 r^2. \end{aligned} \tag{5.46}$$

Considering only the state r, the equilibria are determined by

$$\dot{r} = 0 = r_{eq}(d\mu + j_0 r_{eq}^2); \tag{5.47}$$

therefore, the equilibria are

$$r_{eq} = 0, \sqrt{-\frac{d\mu}{j_0}}. \tag{5.48}$$

The equilibrium at the origin will always exist, but the second equilibrium will only exist if $\frac{d\mu}{j_0} < 0$.

For the second equilibrium, all that is necessary for a periodic orbit is that $\dot{\theta}$ be non-zero. Since ω is a constant independent of μ, this will always be the case.

Since the radius depends only on constants, this equilibrium will correspond to a periodic orbit at this radius. Let $r^* = \sqrt{-\frac{d\mu}{j_0}}$, and perform the change of coordinated $\rho = r - r^*$. The dynamics in ρ are given by

$$\begin{aligned}
\dot{\rho} = \dot{r} &= 2r(d\mu + j_0 r^2) \\
&= j_0 r \left(\frac{d\mu}{j_0} + r^2 \right) = j_0 r \left(r^2 - r^{*2} \right) \\
&= a\rho(\rho + r^*) \left(\rho + 2r^2 \right).
\end{aligned} \tag{5.49}$$

The stability can be tested via the Lyapunov direct method with candidate function $V = \frac{1}{2}\rho^2$. If

$$\begin{aligned}
\dot{V} = \rho\dot{\rho} &= j_0\rho^2(\rho + r^*)(\rho + 2r^*) \\
&= j_0\rho^2(\rho^2 + 3r^*\rho + 2r^*) \\
&= 2j_0 r^*\rho^2 + 3j_0 r^*\rho^3 + j_0\rho^4
\end{aligned} \tag{5.50}$$

is negative definite, then V is a Lyapunov function. For ρ sufficiently small near zero, the second order term of (5.50) will dominate; the periodic orbit will then be stable locally if $j_0 < 0$.

Now consider the origin's stability through the Lyapunov function $V = \frac{1}{2}r^2$. This will result in

$$\dot{V} = r\dot{r} = d\mu r^2 + j_0 r^4. \tag{5.51}$$

Once again, the second order term dominates locally near the origin, and the

origin will be stable if $d\mu < 0$, or at $\mu = 0$ if $j_0 < 0$

To summarize, the possible cases categorized by d and j_0 are:

Case 1: $d > 0$, $j_0 > 0$

Origin: Unstable for $\mu \geq 0$; asymptotically stable for $\mu < 0$

Periodic Orbit: Unstable for $\mu < 0$; otherwise non-existent

Case 2: $d > 0$, $j_0 < 0$

Origin: Unstable for $\mu > 0$; asymptotically stable for $\mu \leq 0$

Periodic Orbit: Asymptotically stable for $\mu > 0$; otherwise non-existent

Case 3: $d < 0$, $j_0 > 0$

Origin: Unstable for $\mu \leq 0$; asymptotically stable for $\mu > 0$

Periodic Orbit: Unstable for $\mu > 0$; otherwise non-existent

Case 4: $d < 0$, $j_0 < 0$

Origin: Unstable for $\mu > 0$; asymptotically stable for $\mu \leq 0$

Periodic Orbit: Asymptotically stable for $\mu < 0$; otherwise non-existent

If one considers the stability of the periodic orbit in terms of the coefficient j_0 then there are two options. For $j_0 < 0$ it is possible for the periodic orbit to exist: (Case 2) for $\mu > 0$ or (Case 4) for $\mu < 0$. In both cases the orbit is asymptotically stable. Conversely, for $j_0 > 0$ the periodic orbit can exist for $\mu > 0$ (Case 3) or $\mu < 0$ (Case 1), but in both cases the periodic orbit is unstable. The coefficient j_0 is an indicator of whether the bifurcating periodic orbit is stable ($j_0 < 0$), the *supercritical* bifurcation, or unstable ($j_0 > 0$), the *subcritical* bifurcation.

Ignoring the higher order terms, the system is shown to have an equilibrium at the origin, and it may have a periodic orbit. With the higher order terms the dynamics can be verified to remain the same; i.e., for μ sufficiently small the dynamics described by truncated form will still hold [19].

We will offer a justification of a stable periodic orbit in case 2 with $\mu > 0$ for the full system. Choose $\mu > 0$ sufficiently small and consider the annulus shown

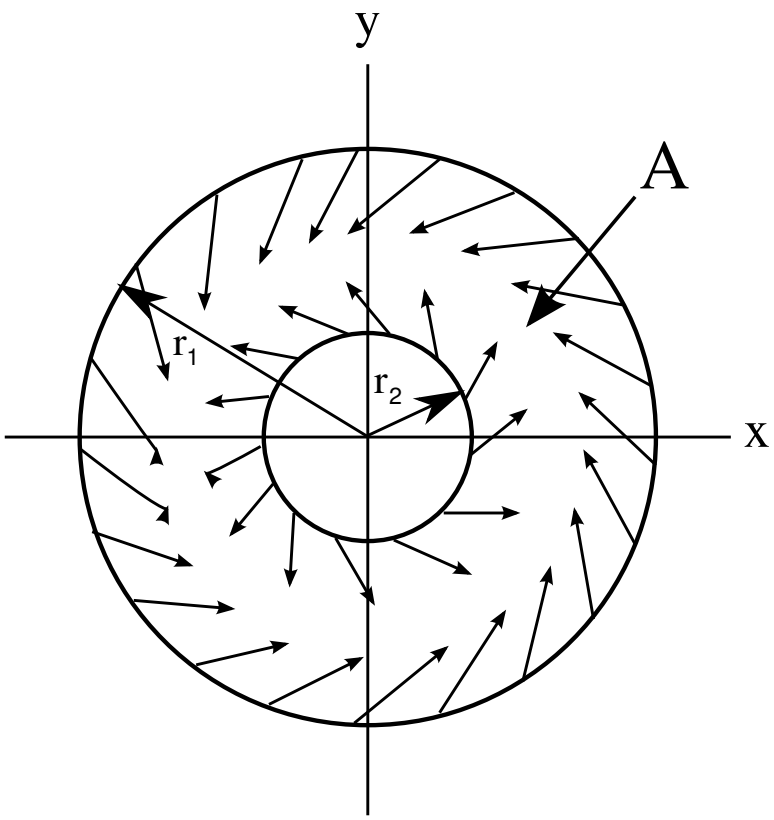

Figure 5.1: The annulus contains the limit cycle but no fixed point.

in Figure 5.1, described by

$$A = \{(r, \theta) | r_1 \leq r \leq r_2\}, \tag{5.52}$$

where r_1 and r_2 are chosen such that

$$0 < r_1 < \sqrt{\frac{-d\mu}{j_0}} < r_2. \tag{5.53}$$

On the boundary of A, at r_2, the vector field given by the truncated normal form (5.46) will have an $\dot{r} < 0$; therefore, the vector field is pointing strictly into the interior of A. A is a positive invariant region, so A contains the stable periodic orbit and no fixed points.

Examining the properties of the Hopf bifurcation shows that there exists an equilibrium and that there may exist a periodic orbit. The stability of these will

depend on the parameters.

Considering the full normal form (5.45), with μ and r sufficiently small, the $\mu^2 r$, μr^3, and r^5 terms can be made smaller than the rest; therefore, if r_1 and r_2 are also taken sufficiently small, then the annulus A will still be a positive invariant region containing no fixed points. By the Poincaré-Bendixon theorem, A contains a stable periodic orbit. The three other cases can be handled in the same way with the exception of the cases where $j_0 > 0$, when the time-reversed flow must be utilized. For the full proof see [20].

CHAPTER 6

SOLITONS AS A CONTROL PROBLEM

In Chapter 2 a second order ODE was derived that describes the pulse propagation as it travels through the fiber. The first step is to convert the ODE into a set of states and an input. Then this ODE simply looks like a nonlinear system of the form

$$\dot{x} = f(x, u). \tag{6.1}$$

Control theory has tools specifically designed to deal with systems of this type. Converting (2.63) to the appropriate state representation results in

$$\begin{aligned} \dot{a}_1 &= a_2, \\ \dot{a}_2 &= \frac{\beta_2^2}{a_1^3} + \frac{\beta_2 \kappa a_0}{a_1^2}, \end{aligned} \tag{6.2}$$

where a_1, a_2 are states corresponding to the pulse width (a) and chirp (a_z), and $\dot{a_1}$ denotes the derivative of a with respect to the *space* variable z. The dispersion β_2 will be the input u. Figure 6.1 shows the corresponding closed-loop block diagram.

A soliton solution to this ODE propagates with no change in width. This

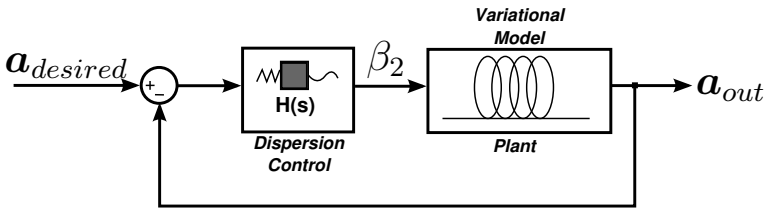

Figure 6.1: Controlled dispersion management. Full-state feedback is applied to the plant to continuously modify the dispersion map.

would correspond to a stable fixed point at the desired soliton width. Since a fixed point will only exist if $a_2 = 0$ at the equilibrium, let the fixed point be described by $(a_{eq}, 0)$. To analyze this fixed point, change coordinates to move the equilibrium to the origin according to $x_1 = a_1 - a_{eq}$, $x_2 = a_2$, which results in the system

$$\begin{aligned} \dot{x}_1 &= f_1(x) = x_2 \\ \dot{x}_2 &= f_2(x) = \frac{\beta^2}{(x_1 + a_0)^3} + \frac{\beta \kappa a_0}{(x_1 + a_0)^2}, \end{aligned} \tag{6.3}$$

where β_2 has been replaced by β, accounting for the shift in coordinates.

For $(a_{eq}, 0)$ to be an equilibrium, the condition $f_2(0) = 0$ must hold, which will only be the case with the correct input. Let β be a function of both x_1 and x_2, and consider the Taylor series expansion of β around $x = (0, 0)$ given by

$$\begin{aligned} \beta_{i\,k}(x) &= \left. \frac{\partial^{i+k} \beta(x)}{\partial x_1^i \, \partial x_2^k} \right|_{x=0} \\ \beta &= \sum_{i,k=0}^{\infty} \beta_{ik} x_1^i x_2^k. \end{aligned} \tag{6.4}$$

The condition for a fixed point at the origin is then

$$f_2(0) = 0 = \frac{\beta_0^2}{a_{eq}^3} + \frac{\beta_0 \kappa a_0}{a_{eq}^2}. \tag{6.5}$$

This is equivalent to a condition on the input signal,

$$\beta_0 = -\kappa a_0 a_{eq}. \tag{6.6}$$

Now that an equilibrium at the origin has been obtained, control must be applied such that stable solitons are created. We consider two types of solitons, those with and without chirp, i.e., $a_{z,eq} \neq 0$ and $a_{z,eq} = 0$, at the desired equilibrium.

6.1 No Chirp Soliton

From (6.3) a soliton in this framework cannot exist with chirp. The fixed point must be of the form $(a_{eq}, 0)$, and if the a_2 component is non-zero there will not be a fixed point. If the desired soliton does not have a chirp component, this is not a problem. Creating a soliton corresponds to guaranteeing that the fixed point is asymptotically stable. Let the fixed point coincide with the initial conditions, i.e., $a_0 = a_{eq}$.

The stability of the fixed point is determined through the application of the Lyapunov indirect method. If the eigenvalues of the Jacobian,

$$J = \begin{bmatrix} 0 & 1 \\ J_{12} & J_{22} \end{bmatrix}, \tag{6.7}$$

where

$$J_{12} = -\kappa\left(\kappa + \frac{1}{a_0}\beta_{10}\right) \text{ and } J_{22} = -\frac{\kappa}{a_0}\beta_{01} \tag{6.8}$$

evaluated at the equilibrium $(a_0, 0)$, are in the open left half-plane, then the full nonlinear system is stable [21]. The eigenvalues of (6.7) are

$$\lambda_{1,2} = \frac{1}{2}J_{22} \pm \sqrt{\frac{J_{22}^2}{4} + J_{12}} \tag{6.9}$$

These eigenvalues depend on β_{01} and β_{10}, so the complex pole pair can be arbitrarily placed in the complex plane at a point p and its complex conjugate, such that the eigenvalues are $\mathrm{Re}\{p\}\pm\mathrm{Im}\{p\}$. The control conditions are

$$\begin{aligned} \beta_{01} &= -\frac{2a_0}{\kappa}\mathrm{Re}\{p\}, \\ \beta_{10} &= \frac{\kappa}{4a_0}\beta_{01}^2 - \frac{a_0}{\kappa}\left(1 + |\mathrm{Im}\{p\}|^2\right). \end{aligned} \tag{6.10}$$

The eigenvalues are placed by first setting their real part, and after determining β_{01}, setting their imaginary part.

The control law will then be linear of the form

$$\beta_2 = \beta_0 + \beta_{10}(a - a_0) + \beta_{01}a_z. \tag{6.11}$$

This control law will create a stable fixed point at the desired position assuming the closed-loop eigenvalues are selected such that the real part is in open left half complex plane.

6.2 Chirped Soliton

In this case the desired soliton corresponds to a stable fixed point at $(a_{eq}, a_{z,eq})$. This is impossible as a fixed point cannot have a a_z component due to the form of $f_1(x)$. It is clear that control cannot create a soliton at the desired fixed point. A solution is to produce a pulse that, on average, experiences no dispersion, as in the dispersion managed case. The pulse will periodically return to the desired state.

This solution corresponds to a periodic orbit of the dynamical system. It is advantageous for the periodic orbit to be stable so that disturbances do not cause the pulse to be lost. This is equivalent to a stable limit cycle. One example of a stable limit cycle is the supercritical Hopf bifurcation as described in Chapter 5. If there exists a transformation such that the system (6.3) can be put into a Hopf bifurcation normal form, then we will have achieved our goal. The control will be designed to ensure that the closed-loop system exhibits a supercritical Hopf bifurcation in the normal form. This approach is similar in spirit to the idea of controlled bifurcation explored, e.g., in [22].

From normal form theory, the normal form is determined by the eigenvalues of the Jacobian. To obtain a Hopf bifurcation, the Jacobian at $(a_{eq}, 0)$ must have eigenvalues of the form $\alpha(\mu) \pm i\omega(\mu)$ with $\alpha(0) = 0$ and $\omega(0) \neq 0$.

From Chapter 4 the next step is to transform the system so that the Jacobian is in real Jordan form. Rather than transform our soliton system, which would

complicate determining the desired control, we will transform the Hopf normal form such that the linear part matches our system (6.3):

$$\dot{z} = G(z, 0) \tag{6.12}$$

of the form

$$\begin{aligned} \dot{z_1} &= z_2 + \left(j_0 z_1 + \frac{k_0}{\omega_0} z_2 \right) (\omega_0^2 z_1^2 + z_2^2) + \mathcal{O}(5) \\ \dot{z_2} &= -\omega_0^2 z_1 + (j_0 z_2 - k_0 \omega_0 z_1)(\omega_0^2 z_1^2 + z_2^2) + \mathcal{O}(5), \end{aligned} \tag{6.13}$$

which is obtained from (5.41) through the transform

$$z_1 = \frac{1}{\omega_0} y_2 \text{ and } z_2 = y_1.$$

The function $G(z, \mu)$ is equivalent to the resonant terms $F^r(y)$ from Chapter 4. This will allow us to use these coefficients in determining the transformation into normal from and the equivalence between variables in the soliton system and coefficients of the Hopf normal form.

For the first order terms, since the relationship is now one to one,

$$\begin{aligned} \alpha(\mu) &= \frac{1}{2} J_{22}, \text{ and} \\ \omega(\mu) &= \sqrt{-J_{12} - \frac{J_{22}^2}{4}} \ . \end{aligned} \tag{6.14}$$

Since μ is the bifurcation parameter which should be controlled, let $\beta_{01} = \mu$; then

$$\beta_{10} = \frac{a_0}{\kappa} (\omega_0^2 - \kappa^2). \tag{6.15}$$

For the second order transformation, the homological equation is

$$G_2(y) = J\Gamma_2(y) - \nabla\Gamma_2(y) J y + F_2(y). \tag{6.16}$$

The function $G_2(y)$ can be described in terms of the Taylor series by its coefficients, namely

$$G_2(y) = \begin{pmatrix} g_{20}y_1^2 + g_{11}y_1y_2 + g_{02}y_2^2 \\ G_{20}y_1^2 + G_{11}y_1y_2 + G_{02}y_2^2 \end{pmatrix}, \tag{6.17}$$

and likewise

$$\Gamma_2(y) = \begin{pmatrix} h_{20}y_1^2 + h_{11}y_1y_2 + h_{02}y_2^2 \\ H_{20}y_1^2 + H_{11}y_1y_2 + H_{02}y_2^2 \end{pmatrix}. \tag{6.18}$$

Applying this convention results in six equations that describe the coefficients of G_2. Substituting the equivalent values for the coefficients from the known form of F_2 (6.3) gives the linear equation

$$\begin{bmatrix} 0 & \omega_0^2 & 0 & 1 & 0 & 0 \\ -2 & 0 & 2\omega_0^2 & 0 & 1 & 0 \\ 0 & -1 & 0 & 0 & 0 & 1 \\ -\omega_0^2 & 0 & 0 & 0 & \omega_0^2 & 0 \\ 0 & -\omega_0^2 & 0 & -2 & 0 & 2\omega_0^2 \\ 0 & 0 & -\omega_0^2 & 0 & -1 & 0 \end{bmatrix} \begin{bmatrix} h_{20} \\ h_{11} \\ h_{02} \\ H_{20} \\ H_{11} \\ H_{02} \end{bmatrix} = \begin{bmatrix} g_{20} \\ g_{11} \\ g_{02} \\ G_{20} + \frac{\omega_0^4 + 2\omega_0^2\kappa^2 + \beta_{20}\kappa^3}{a_0\kappa^2} \\ G_{11} \\ G_{02} \end{bmatrix}. \tag{6.19}$$

From the Hopf normal form, all second order terms should cancel, resulting in $G_2(y) = 0$. Since the linear equation (6.19) is of the form $Ax = b$ with A of full rank, all the second order terms of G can be set to zero; in addition, we can set $\beta_{20} = \beta_{02} = 0$. Solving the system yields the second order terms of the transformation,

$$\begin{bmatrix} h_{20} \\ h_{11} \\ h_{02} \\ H_{20} \\ H_{11} \\ H_{02} \end{bmatrix} = \begin{bmatrix} \frac{1}{3}\frac{\omega_0^2 + 2\kappa^2}{a_0\kappa^2} \\ 0 \\ \frac{2}{3}\frac{\omega_0^2 + 2\kappa^2}{a_0\kappa^2\omega_0^2} \\ 0 \\ -\frac{2}{3}\frac{\omega_0^2 + 2\kappa^2}{a_0\kappa^2} \\ 0 \end{bmatrix}. \tag{6.20}$$

The third order Hopf normal form determines the radius and frequency of the periodic orbit, so the transform must be computed to at least third order. At this order, the homological equation results in eight equations. In terms of the coefficients of the transformation, the linear system is $Ax = b$ of the form

$$\begin{bmatrix} 0 & \omega_0^2 & 0 & 0 & 1 & 0 & 0 & 0 \\ -3 & 0 & 2\omega_0^2 & 0 & 0 & 1 & 0 & 0 \\ 0 & -2 & 0 & 3\omega_0^2 & 0 & 0 & 1 & 0 \\ 0 & 0 & -1 & 0 & 0 & 0 & 0 & 1 \\ -\omega_0^2 & 0 & 0 & 0 & 0 & \omega_0^2 & 0 & 0 \\ 0 & -\omega_0^2 & 0 & 0 & -3 & 0 & 2\omega_0^2 & 0 \\ 0 & 0 & -\omega_0^2 & 0 & 0 & -2 & 0 & 3\omega_0^2 \\ 0 & 0 & 0 & -\omega_0^2 & 0 & 0 & -1 & 0 \end{bmatrix} \begin{bmatrix} h_{30} \\ h_{21} \\ h_{12} \\ h_{03} \\ H_{30} \\ H_{21} \\ H_{12} \\ H_{03} \end{bmatrix} =$$

$$\begin{bmatrix} g_{30} + \frac{\kappa\beta_{03}}{a_0} \\ g_{21} \\ g_{12} \\ g_{03} \\ G_{30} + \frac{\omega_0^4\kappa^2 + \omega_0^2\kappa^4 + 3\kappa^5 a_0\beta_{30} - 2\omega_0^6}{3a_0^2\kappa^4} \\ G_{21} \\ G_{12} - \frac{16\kappa^4 + 16\omega_0^2\kappa^2 + 4\omega_0^4}{3a_0^2\kappa^4} \\ G_{03} \end{bmatrix}. \tag{6.21}$$

The matrix A is of rank six, and solving (6.21) requires the use of the Fredholm

alternative. After computing

$$Ker(A^*) = span\left\{\begin{bmatrix} 3 \\ 0 \\ \omega_0^2 \\ 0 \\ 0 \\ 1 \\ 0 \\ 3\omega_0^2 \end{bmatrix}, \begin{bmatrix} 0 \\ \omega_0^2 \\ 0 \\ 3\omega_0^4 \\ -3 \\ 0 \\ -\omega_0^2 \\ 0 \end{bmatrix}\right\}, \tag{6.22}$$

the vector b must be orthogonal to both vectors spanning this space. Since the final form desired is (6.13), the second order g_{ik} and G_{ik} terms can be substituted for their counterparts. This gives two equations for determining the values of the third order control based on the desired values of j_0 and k_0 of (5.41);

$$\begin{aligned} \beta_{03} &= -\frac{8a_0}{3\kappa} j_0 \text{ and} \\ \beta_{30} &= \frac{24\omega_0^2 a_0^2 \kappa^2 k_0 - 19\omega_0^2\kappa^2 + 13\kappa^4 + 2\omega_o^4}{9\kappa^5 a_0}. \end{aligned} \tag{6.23}$$

Since the control has created a Hopf bifurcation, the coefficient must be chosen such that a supercritical bifurcation occurs and matches the desired periodic orbit.

The desired soliton has the parameters $(a_{eq}, a_{z,eq})$, since the fixed point can only be set on the real axis. The best solution is to set the fixed point directly below the desired pulse parameters as shown in Figure 6.2. Then making the radius $r = a_{z,eq}$, which is valid up to second order, guarantees that the limit cycle passes through the desired pulse characteristic once a period. To simplify, the desired pulse parameters will be the initial condition of the pulse,

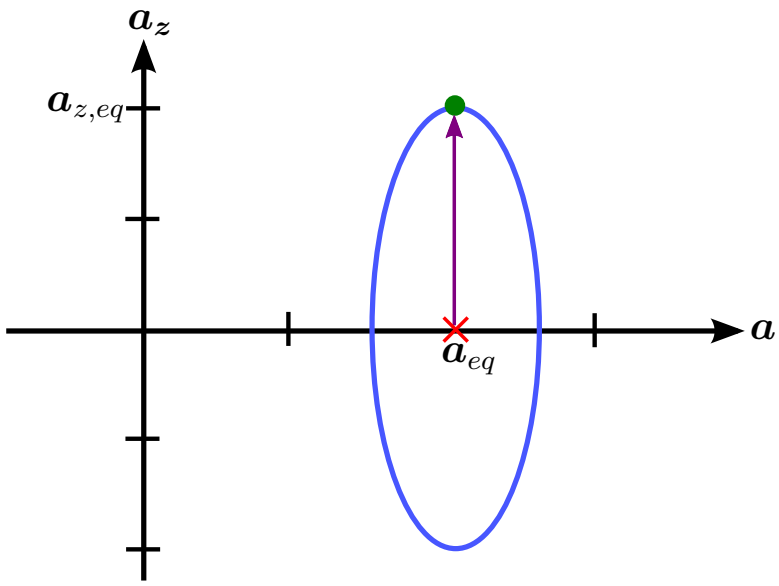

Figure 6.2: Limit cycle in phase space. The limit cycle passes through the desired initial conditions.

$(a_{eq}, a_{z,eq}) = (a_0, a_z(0))$. This requires the condition

$$\beta_0 = -\kappa a_0^2. \tag{6.24}$$

The coefficients must be chosen such that a stable limit cycle is created. The conditions for a supercritical Hopf are:

1. $\mu > 0$
2. $j_0 < 0$
3. $d < 0$

Notice that there are five parameters describing the system $(j_0, k_0, \omega_0, d, \mu)$ and three equations for the system (the radius, frequency, and center).

Consider the frequency of the periodic orbit (5.46)

$$\dot{\theta} = \omega_0 + j_0\mu + k_0 r^2; \tag{6.25}$$

the frequency can be split into two components, ω_0 and $j_0\mu + k_0 r^2$. The desired

frequency is the $\Omega = \dot{\theta} = \frac{2\pi}{L}$, where L is the fiber length. The first order terms of Ω, i.e. ω_0, should dominate; the second order terms are more likely to fluctuate in response to disturbances. Let $\omega_0 = 0.9\Omega$, resulting in the control

$$\beta_{10} = \left(\omega_0^2 - \kappa^2\right) \frac{a_0}{\kappa}. \tag{6.26}$$

There is still a free parameter, so choose a $j_0 < 0$. From (5.48) the radius in terms of the actual system coefficient is

$$r = a_z(0) = \sqrt{-\frac{d\mu}{j_0}} = \sqrt{-\frac{J_{22}}{2j_0}} = \sqrt{\frac{\kappa}{2a_0 j_0}\beta_{01}}. \tag{6.27}$$

Solving for the desired control yields

$$\beta_{01} = \mu = 2r^2 j_0 \frac{a_0}{\kappa}. \tag{6.28}$$

Now solve for k_0 from the remaining frequency component of (6.25):

$$k_0 = 0.2\Omega \frac{a_0 j_0}{\kappa \beta_{01}}. \tag{6.29}$$

From (6.23) solving for the remaining control coefficients yields

$$\beta_{03} = -\frac{8 j_0 a_0}{3\kappa}, \tag{6.30}$$

$$\beta_{30} = \frac{24\omega_0^3 a_0^2 \kappa^4 k_0 + 13\omega_0^2\kappa^4 + 13\omega_0^4\kappa^4 + 10\omega_0^6}{9 a_0 \kappa^5}. \tag{6.31}$$

The free parameters can be adjusted. If the fiber's dispersion input is bounded (that is, if we know a priori that $|\beta(a, a_z)| < M$ for some region of space), a trial and error process can be used to find an appropriate j_0 such that the control input satisfies them. Also the splitting of (6.25) can be performed differently to satisfy constraints that might be placed on the control.

To summarize, we have devised control laws to create a soliton pulse with no chirp and a pulse that experiences the soliton effect, either exactly or on

average, for pulses that require a particular chirp.

6.3 Estimating Uncertain Parameters

In developing the control laws, the parameters a_0, P_0, and γ are assumed to be constant and known. While a_0 and P_0 correspond to initial conditions that can be precisely controlled, γ is dependent upon the fiber and, due to manufacturing, may vary across the fiber within some tolerance. Since the control law requires knowledge of the value of γ, implementation will necessitate an estimation of nonlinearity.

Traditional control techniques involve online adaptation that continuously updates the estimate such that the error between the real parameter and the estimate converges to zero. This approach fails in this system as it is impossible to distinguish between the uncertain parameter and the input. It is then impossible to construct a Lyapunov equation that will guarantee convergence. To overcome this limitation, by thinking of the problem as an infinite family of plants, the problem is reduced to determining the plant that is running and then applying the proper control for the plant. This type of problem falls under hybrid control theory, which estimates the running process through logic based switching.

The technique we will use is inspired by *supervisory control* design as described by [23]. To better illustrate the technique, (6.3) is put in the standard form

$$\begin{aligned} \dot{x}_1 &= x_2 \\ \dot{x}_2 &= \frac{u^2}{(x_1 + a_0)^3} + \gamma \frac{u P_0 a_0}{\sqrt{2}(x_1 + a_0)^2}. \end{aligned} \tag{6.32}$$

To illustrate the connection to hybrid control, the plant (6.32) can be thought of as a family of plants parameterized by $\gamma \in \mathbb{R}_{>0}$, to which corresponds a family of controllers also parameterized by γ. Then γ is estimated by determining the

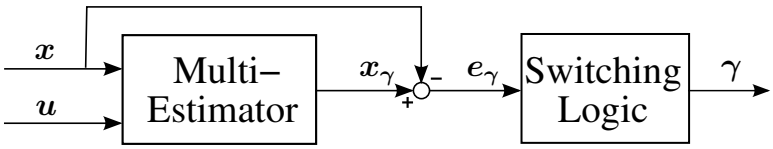

Figure 6.3: The block diagram of the supervisor control system.

current plant that is running and choosing the appropriate controller.

The subset of supervisory control we will use will consist of two subsystems, a multi-estimator and switching logic, as shown in Figure 6.3. The multi-estimator provides estimates of the family of plants using the states of the running plant and the applied input. The switching logic differentiates between the plants and makes the final determination of which plant is running. In this case the output of the switching logic will be the estimate of the parameter γ.

The multi-estimator is a dynamical system whose inputs are the input u and the state x of the plant. The output signals x_γ are a family of signals generated by applying each $\gamma \in \mathbb{R}_{>0}$. This family of signals provide approximations of x regardless of the input. A natural requirement for the system is that x_γ converge to x asymptotically for all $\gamma \in \mathbb{R}_{>0}$, if the physical plant is equal to the nominal process model with no noise or disturbance [24]. This is equivalent to the asymptotic convergence of the estimation error,

$$e_\gamma = x_\gamma - x, \, \forall \gamma \in \mathbb{R}_{>0}, \tag{6.33}$$

to zero.

In our system the uncertainty enters the system only in x_2. This will be the estimated state of the multi-estimator; the input u will be the control input β. If the estimator equation is

$$\dot{x}_\gamma = -K(x_\gamma - x_2) + \frac{u^2}{(x_1 + a_0)^3} + \gamma \frac{uP_0}{\sqrt{2}(x_1 + a_0)^2}, \, \forall \gamma \in \mathbb{R}_{>0} \tag{6.34}$$

then the estimation error (6.33) satisfies $\dot{e}_\gamma = -Ke_\gamma \; \forall \gamma \in \mathbb{R}_{>0}$, where K is an appropriately chosen gain. By choosing K the error will converge to zero

exponentially fast, for an arbitrary control input u.

Implementing the multi-estimator as a parallel connection of individual estimators for all possible values of γ is not efficient and is actually impossible for the infinite set $\gamma \in \mathbb{R}_{>0}$ [24]. Fortunately, the idea of *state sharing*, which allows all estimators to be replaced by a single estimator, can be applied. State sharing is always possible if the estimator equations are "affinely separable" in the unknown parameters, as in $\dot{x}_p = -\lambda x_p + f_1(p) f_2(x, u)$ [24]. Applying this results in

$$\begin{aligned} \dot{z}_1 &= -z_1 + x_2 + \frac{u^2}{(x_1 + a_0)^3} \\ \dot{z}_2 &= -z_2 + u\frac{P_0 a_0}{\sqrt{2}(x_1 + a_0)^2}, \end{aligned} \tag{6.35}$$

and the output is

$$x_\gamma = z_1 + \gamma z_2. \tag{6.36}$$

Computing $\dot{x}_\gamma$ will show the two are equivalent.

The switching logic must differentiate between the estimates and determine the best estimate. In the fiber system the nonlinearity γ will vary continuously and thus no constraints on the switching of the estimate state are required. It is clear that the best estimate will be the one in which the error squared is a minimum. The error is $e_\gamma = z_1 + \gamma z_2 - x_2$, and the error squared is

$$e_\gamma^2 = (x_\gamma - x)^2 = (z_1 - x_2)^2 + 2\gamma z_2 (z_1 - x_2) + \kappa^2 z_2^2. \tag{6.37}$$

Seeking to minimize the function with respect to γ, we differentiate (6.37) to obtain

$$\begin{aligned} &\frac{\partial e_\gamma^2}{\partial \gamma} = 2z_2(z_1 - x_2) + 2\gamma z_2^2, \text{ and} \\ &\frac{\partial^2 e_\gamma^2}{\partial \gamma^2} = 2z_2^2. \end{aligned} \tag{6.38}$$

The second derivate is $z_2^2 > 0$ and thus the error squared is a convex function of γ. The necessary and sufficient condition for a minimum is then

$$0 = \frac{\partial e_\gamma^2}{\partial \gamma} = 2z_2(z_1 - x_2) + 2\gamma z_2^2. \tag{6.39}$$

Solving for γ yields

$$\gamma = -\frac{z_1 - x_2}{z_2}. \tag{6.40}$$

Since the function is convex with respect to γ, the critical point is a minimum, making it the best estimate for γ.

Using the estimate

$$\hat{\gamma} = -\frac{z_1 - x_2}{z_2} \tag{6.41}$$

will result in modifying the control laws by replacing κ with

$$\hat{\kappa} = \frac{\hat{\gamma} P_0}{\sqrt{2}} = \frac{(x_2 - z_1)P_0}{z_2\sqrt{2}}. \tag{6.42}$$

This control law is simulated in Chapter 7 and is shown to result in convergence to a limit cycle and the correct value of the parameter γ if the nonlinearity is unknown but constant.

CHAPTER 7

SIMULATIONS

In this chapter, we illustrate through simulations the advantages of the feedback control strategy introduced in Chapter 6 over current techniques, such as DM.

All simulations are conducted on the variational model (6.3). A constant energy source of 1 ps·W is used, so as the pulse width decreases, the initial power increases. We use a Kerr nonlinearity of $\gamma = 1$ (km·mW)$^{-1}$. These are rough estimates for real values, but they will demonstrate the various systems' properties.

The baseline system is an optical fiber with a constant positive dispersion map with a typical value of β_2, 2 ps^2/km. As seen in Figure 7.1 the dispersion and nonlinearity cause the pulse width to increase unchecked, requiring retransmission whenever the pulse width goes beyond a certain tolerance. Also notice that the longer pulse widths have less spreading, which is why fiber optics today generally use this inexpensive method for short distances.

The current technology of choice for soliton propagation is dispersion management. This control is essentially open-loop and relies on estimating the fiber's properties well enough to match the proper lengths of positive and negative dispersion fiber. For this simulation the positive fiber has a length L_1 of 50 km and β_2 of 2 ps^2/km. It is followed by a length L_2 of 10 km of negative dispersion fiber of β_2 = -20 ps^2/km. This setup is repeated for the full length of the fiber. The dispersion management system causes the pulse width to have a periodic orbit for the larger pulse widths (see Figure 7.2). At the shorter pulse widths, specifically 10 ps, the nonlinearity is too large and cannot be compensated for, causing the pulse width to become unstable.

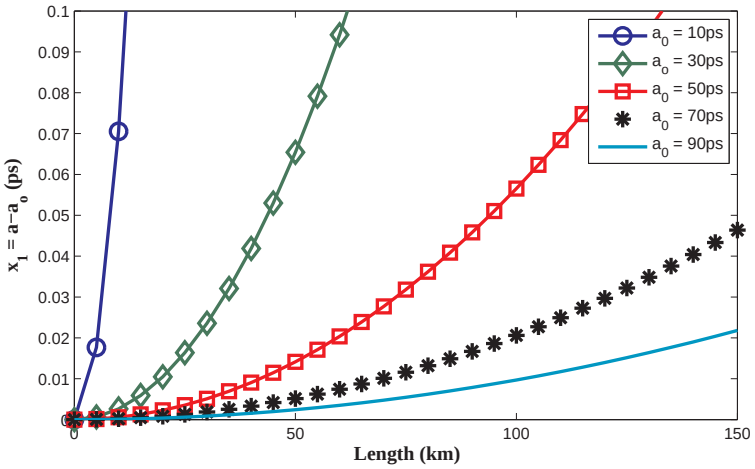

Figure 7.1: Pulse width evolution in an uncontrolled fiber (β_2 = constant).

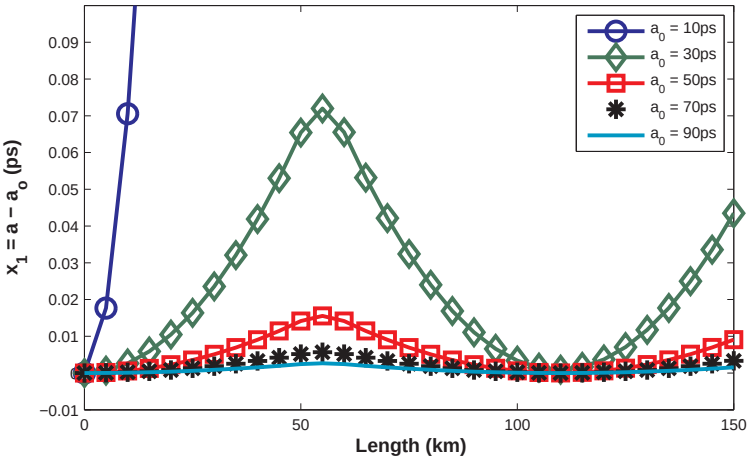

Figure 7.2: Simulated dispersion management. The scheme fails to generate a periodic behavior at lower pulse widths.

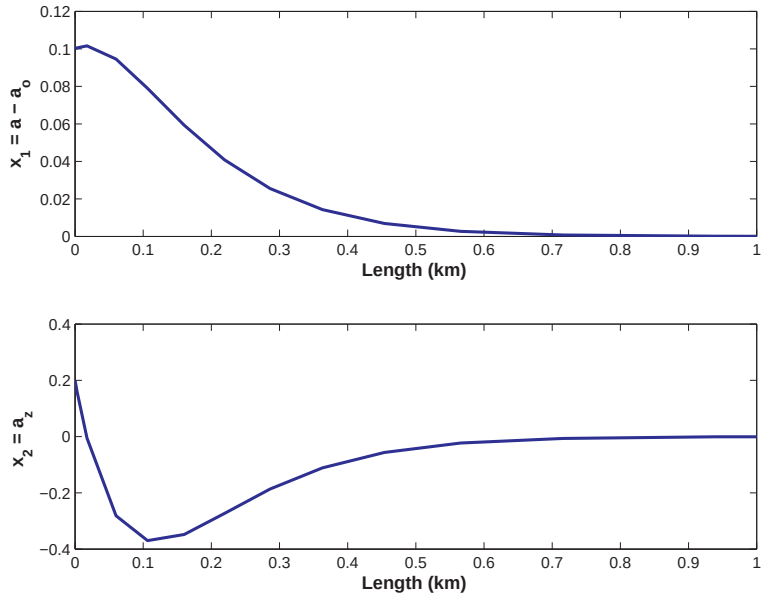

Figure 7.3: Stable fixed point soliton control.

If the controlled system proposed can propagate the 10 ps pulses under high nonlinearity, then it will have demonstrated its advantage over the current technology. Consider first a soliton with no chirp with the parameter $a_{eq} = 10$ ps. The additional advantage of feedback control is disturbance rejection. Applying the wrong initial conditions $(10.1, 0.2)$ will demonstrate this property. The closed-loop eigenvalues are set to -10 rad/s. In Figure 7.3 the control system brings the system to the desired parameters after a small transient. After 1 km the stable state has been reached and the soliton propagates without fluctuation.

To demonstrate the chirped soliton, the desired parameters are set to $(a_o, a_z(0)) = (10, 0.01)$. The system is designed with the following parameters for the closed-loop limit cycle: radius $r = 0.01$ ps, length $L = 10$ km, and $j_0 = -10$. In order to verify that the limit cycle exists locally, the initial conditions must be near the orbit, but to demonstrate disturbance rejection the input pulse will be (10.1 ps, 0.09 ps/km), which is larger than desired. In Figure 7.4 the 10 ps pulse experiences a periodic orbit and does not increase beyond the deviation allowed by the radius of the limit cycle. Once per period, the pulse returns to its original shape. The limit cycle is clearly observed, as the original deviation

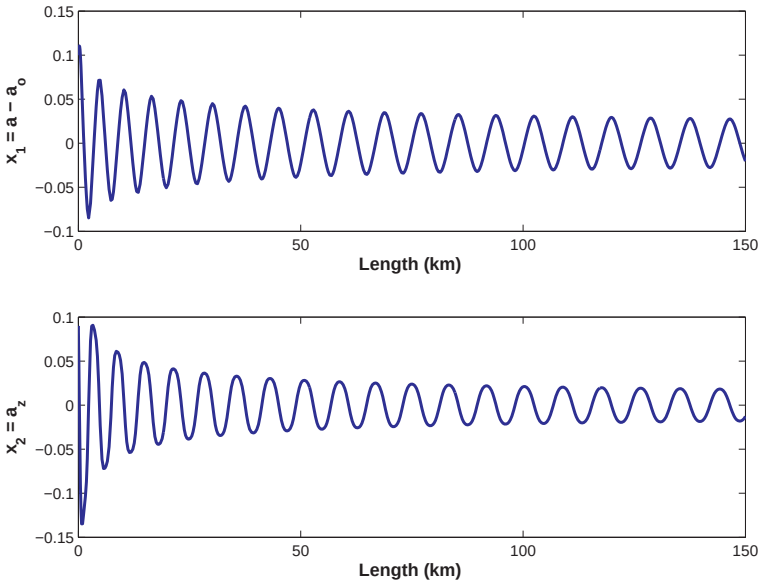

Figure 7.4: Limit cycle obtained with controlled dispersion. Both states converge to periodic orbits, even for very short initial pulse width.

asymptotically converges to the desired periodic orbit.

The control laws with no uncertainty create the desired soliton solutions. Adding in the estimator for γ will introduce uncertainty. The nonlinearity is assumed constant as before $\gamma = 1$ $(\text{km}\cdot\text{mW})^{-1}$, but unknown. Setting the gain $K = 1$, Figure 7.5 shows that the estimate converges to the actual value. The periodic orbits still converge to the limit cycle, but they are slightly deformed due to the uncertainty.

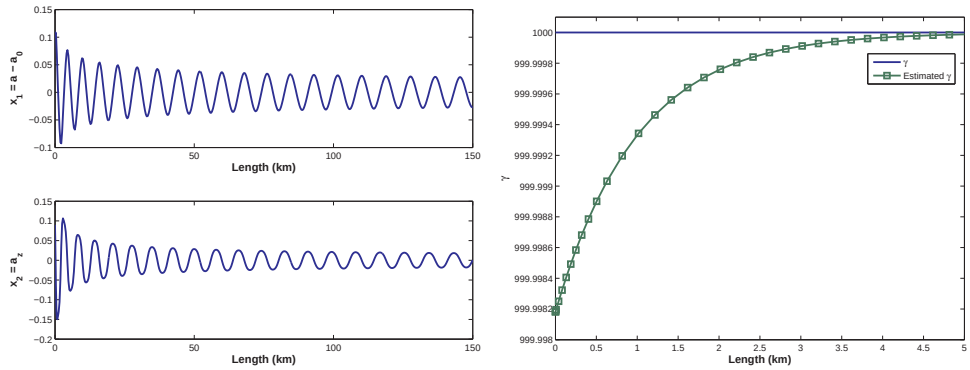

Figure 7.5: Estimator performance. Both states still converge to periodic orbits and the estimate converges to the true parameter.

CHAPTER 8

CONCLUSION AND PERSPECTIVES

The results of the simulation show that solitons of virtually any desired Gaussian shape can be created and propagated through the theoretical fiber we propose. This suggests that it would be advantageous to develop such fibers and apply these control schemes in order to realize extremely high bandwidth optical communication systems. Even if such a fiber were already available, some difficulties would remain in the implementation of our control law. These stem from the simplifying assumptions that were made.

In developing the model, two primary assumptions were made–the SVEA and the weakly guided assumption. As the pulse we are interested in is the Gaussian pulse shape, the SVEA is a good approximation and should be valid for the conditions of interest. It is less clear that the weakly guided assumption remains valid. The pulse width approaches extreme limits; even small variations in the x and y properties in the fiber are in a range comparable to that of the pulse width, so in this case the effects are non-negligible.

For the purposes of theoretical analysis and synthesis of a controller we assumed that the fiber's dispersion could be varied continuously over an infinitesimal region of fiber dz, which is a strong assumption. It would be more realistic to assume that there are discrete lengths of fiber over which the dispersion map can be controlled and constant. This more closely coincides with availability of sensors to measure the pulse width. Such sensors would be finitely arranged over the length of the fiber, not necessarily pairing with each discrete section of dispersion controlled fiber. Designing a controller for this system would involve discretizing the plant and controller such that solitons are still

propagated. We also assumed that the actuators controlling the dispersion would act instantaneously, but in practice delay would be introduced and further complicate the problem.

The framework built in this thesis demonstrates that applying control theory to the propagation of solitons in optical fibers is a worthy goal. This methodology shows great promise for femto-second and smaller pulses required for ultra-high-bandwidth communication channels.

REFERENCES

[1] J. Shaw, *Mathematical Principles of Optical Fiber Communications*. Philadelphia, PA: Society for Industrial Mathematics, 2004.

[2] S. Haykin, *Communication Systems*. New York, NY: Wiley India Pvt. Ltd., 2007.

[3] L. Mollenauer and R. H. Stolen, "The Soliton Laser," *Optics Letters*, vol. 9, pp. 13–15, 1984.

[4] F. Omenetto, A. Taylor, M. Moores, and D. Reitze, "Adaptive control of femtosecond pulse propagation in optical fibers," *Optics Letters*, vol. 26, no. 12, pp. 938–940, 2001.

[5] F. Omenetto, D. Reitze, B. Luce, M. Moores, and A. Taylor, "Adaptive control methods for ultrafast pulse propagation in optical fibers," *IEEE Journal of Selected Topics in Quantum Electronics*, vol. 8, no. 3, pp. 690–698, 2002.

[6] N. Litchinitser, M. Sumetsky, and P. Westbrook, "Fiber-based tunable dispersion compensation," *Journal of Optical and Fiber Communications Research*, vol. 4, no. 1, pp. 41–85, 2007.

[7] G. Agrawal, *Nonlinear Fiber Optics*, 3rd ed. San Diego, CA: Academic Press, 2001.

[8] C. Menyuk, "Application of multiple-length-scale methods to the study of optical fiber transmission," *Journal of Engineering Mathematics*, vol. 36, no. 1, pp. 113–136, 1999.

[9] A. Newell and J. Moloney, *Nonlinear Optics*. Redwood City, CA: Addison-Wesley, 1992.

[10] K. Blow and D. Wood, "Theoretical description of transient stimulated Raman scattering in optical fibers," *IEEE Journal of Quantum Electronics*, vol. 25, no. 12, pp. 2665–2673, 1989.

[11] L. Mollenauer, S. Evangelides Jr., and H. Haus, "Long-distance soliton propagation using lumped amplifiers and dispersion shifted fiber," *Journal of Lightwave Technology*, vol. 9, no. 2, pp. 194–197, 1991.

[12] D. Anderson, "Variational approach to nonlinear pulse propagation in optical fibers," *Physical Review A*, vol. 27, no. 6, pp. 3135–3145, 1983.

[13] M. Brandt-Pearce, I. Jacobs, J. Lee, and J. Shaw, "Optimal input Gaussian pulse width for transmission in dispersive nonlinear fibers," *Journal of the Optical Society of America B*, vol. 16, no. 8, pp. 1189–1196, 1999.

[14] B. Eggleton, J. Rogers, P. Westbrook, and T. Strasser, "Electrically tunable power efficient dispersion compensating fiber Bragg grating," *IEEE Photonics Technology Letters*, vol. 11, no. 7, pp. 854–856, 1999.

[15] J. Brennan, M. Matthews, W. Dower, D. Treadwell, W. Wang, J. Porque, and X. Fan, "Dispersion correction with a robust fiber grating cover the full c-band at 10-gb/s rates with <0.3-dB power penalties," *IEEE Photonics Technology Letters*, vol. 15, no. 12, pp. 1722–1724, 2003.

[16] D. Moss, M. Lamont, S. McLaughlin, G. Randall, P. Colbourne, S. Kiran, and C. Hulse, "Tunable dispersion and dispersion slope compensators for 10 gb/s using all-pass multicavity etalons," *IEEE Photonics Technology Letters*, vol. 15, no. 5, pp. 730–732, 2003.

[17] R. Bise, R. Windeler, K. Kranz, C. Kerbage, B. Eggleton, and D. Trevor, "Tunable photonic band gap fiber," *OSA Trends in Optics and Photonics (TOPS)*, vol. 70, pp. 466–468, 2002.

[18] C. Yu, J. Liou, S. Huang, and H. Chang, "Tunable dual-core liquid-filled photonic crystal fibers for dispersion compensation," *Optics Express*, vol. 16, no. 7, pp. 4443–4451, 2008.

[19] S. Wiggins, *Global Bifurcations and Chaos: Analytical Methods*. New York, NY: Springer-Verlag, 1988.

[20] Y. A. Kuznetsov, *Elements of Applied Bifurcation Theory*. New York, NY: Springer-Verlag, 1998.

[21] H. Khalil, *Nonlinear Systems*, 3rd ed. Englewood Cliffs, NJ: Prentice Hall, 2002.

[22] A. Krener, W. Kang, and D. Chang, "Control bifurcations," *IEEE Transactions on Automatic Control*, vol. 49, no. 8, pp. 1231–1246, 2004.

[23] J. Hespanha, D. Liberzon, and A. Morse, "Overcoming the limitations of adaptive control by means of logic-based switching," *Systems & Control Letters*, vol. 49, pp. 49–65, 2003.

[24] D. Liberzon, *Switching in Systems and Control*. Boston, MA: Birkhauser, 2003.

AUTHOR'S BIOGRAPHY

Thaddeus Egon Koehn was born in Illinois on June 18, 1985. He graduated summa cum laude from the University of Rhode Island in 2006, receiving bachelor of science degrees in electrical engineering, computer engineering, and physics. Before pursuing graduate studies, Thaddeus worked as an electrical engineer in research and development at Electro Standards Labs in Cranston, Rhode Island. During his tenure as a graduate student at the University of Illinois, he met and married Laura Harrison. After graduating in 2009 with a master of science degree in electrical engineering, Thaddeus will begin work at General Dynamics Electric Boat in Groton, Connecticut.